TANAGER: Design and Validation of an Automated Spectrogoniometer for Bidirectional Reflectance Studies of Natural Rock Surfaces

Melissa Rice, Kristiana Lapo, Kathleen Hoza, Ed Cloutis, Mike Kraft, Sean Mulcahy, Dan Applin

Abstract

Laboratory measurements of reflectance spectra of rocks and minerals at multiple viewing geometries are important for interpreting spacecraft data of planetary surfaces. However, efficiently acquiring such measurements is challenging, as it requires a custom goniometer that can accommodate multiple, bulky samples beneath a movable light source and detector. Most spectrogoniometric laboratory work to date has focused on mineral mixtures and particulates, yet it is also critical to characterize natural rock surfaces to understand the influence of texture and alteration. We designed the Three-Axis N-sample Automated Goniometer for Evaluating Reflectance (TANAGER) specifically to rapidly acquire spectra of natural rock surfaces across the full scattering hemisphere. TANAGER has its light source and the spectrometer's fiber optic mounted on motorized rotating and tilting arcs, with a rotating azimuth stage and six-position sample tray, all of which are fully motorized and integrated with a Malvern PanAnalytical ASD FieldSpec4 Hi-Res reflectance spectrometer. Using well-characterized color calibration targets, we have validated the accuracy and repeatability of TANAGER spectra. We also confirm that the system introduces no discernable noise or artifacts. All design schematics and control software for TANAGER are open-source and available for use and modification by the larger scientific community.

1. Introduction

Studying the composition and distribution of minerals on planetary bodies is critical to understanding their surface evolution. Across the solar system, key mineral identifications have been made using visible to near-infrared (VNIR) spectrometers on ground- and space-based telescopes, orbital spacecraft, and landers. VNIR reflectance spectroscopy relies on the analysis of diagnostic absorption features, specifically their band center wavelength positions, shapes, and depths (e.g., Bishop et al., 2020). However, VNIR reflectance spectra are not influenced by mineral composition alone. Variables such as grain morphology (size and shape), temperature, and nonlinear mixing effects also influence the shapes, positions and depths of diagnostic absorption features (e.g., Clark & Roush, 1984; Clark et al., 1999).

In particular, viewing geometry (photometric) effects can complicate remote sensing interpretations. Conversely, once understood, photometric effects can allow for richer inferences to be drawn than would otherwise be possible. For example, photometry has been used to constrain the microtexture of surface materials including roughness and porosity (e.g,. Bandfield et al., 2015; Hapke and Sato, 2016; Shepard et al., 2017). Microtextural characteristics can in turn be used to understand surface processes (e.g., regolith/soil formation and evolution), to serve as inputs to planetary thermal models, and to constrain mechanical properties relevant to exploration. Such investigations have been performed for the Moon (e.g., Shkuratov et al., 1999), asteroids (e.g., Clark et al., 2002), Mars (e.g., Johnson et al., 1999; see also Fernando et al., 2015; Johnson et al., 2006a-b; Johnson et al., 2021, 2022; Lichtenberg et al., 2007) and other planets (e.g., Veverka et al., 1988; Schröder & Keller, 2009). Furthermore, several models have been developed to better understand how the microscale physical properties of surfaces influence photometry (e.g., Hapke, 1993; Shkuratov et al., 1999).

Photometric effects, however, are often not included in laboratory VNIR reflectance measurements of reference rocks and minerals. Many commercial VNIR spectrometers do not allow users to easily control the incidence and emission angles, and most laboratory spectra are acquired with a single, fixed geometry (e.g., incidence = 30°, emission = 0°). In contrast, telescopic and spacecraft observations of planetary surfaces are acquired at a variety of geometries, depending on the relative positions of the light source (Sun), target material (planetary surface), and detector (spectrometer/camera) (e.g., Figure 1). Custom-built goniometers (which control the orientations of the incidence light and spectrometer's detector) are required, therefore, for reproducing photometric effects in the laboratory.

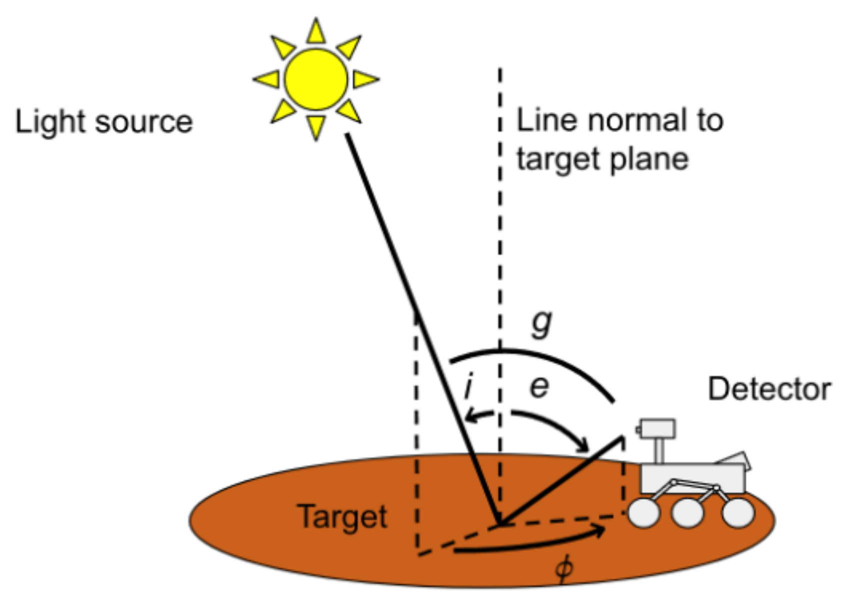

Figure 1. *Cartoon of viewing geometries relevant to spacecraft exploration of planetary surfaces, for the specific example of spectroscopy measurements by a rover on Mars. Geometries shown include emission angle e, incidence angle i, and azimuth angle ϕ. Phase angle g is the angle between e and i.*

To date, such "spectrogoniometry" measurements have focused primarily on particulate samples of uniform grain size and composition (e.g., Pommerol et al., 2013; Shephard and

Helfenstein, 2007) or two-phase mixtures (e.g., Pilorget et al., 2016; Stack & Milliken, 2015). A limited number of laboratory studies have acquired spectrogoniometric measurements for whole rocks (Guinness et al., 1997; Shepherd & Arvidson, 1999). However, the compounding effects of composition, alteration, microtexture, and viewing geometry on complex rock surfaces are still poorly understood. Working with natural rock surfaces in the laboratory poses several challenges. For example, bulky samples require a non-standard goniometer setup with an adjustable sample stage and large incidence and emission arms.

We have designed and built such a system for the Mars Lab at Western Washington University (WWU) in order to characterize the spectrogoniometry of a variety of rock and mineral samples. Specifically, WWU's Mars Lab studies VNIR reflectance spectra of naturally-weathered rocks as analogs to the geologic materials encountered by the Mars Exploration Rovers (MERs), the Mars Science Laboratory (MSL) Curiosity rover, the Mars-2020 Perseverance rover, and future landed missions. The science needs of the Mars Lab necessitate rapid acquisition of spectra from large numbers of bulky samples. For efficiency in collecting large datasets at high angular resolution, it is important to use a motorized system for precise, repeatable positioning of the light source, detector, and sample. Furthermore, software is required to automate the goniometer and allow it to interface with the spectrometer collecting the data. While some aspects of this ideal system have been developed previously for other laboratories (e.g., Biliouris et al., 2007; Camon & Lemelin, 2024; Painter et al., 2003; Pilorget et al., 2016; Pontin et al., 2018; Shepard and Helfenstein, 2007), no fully-automated system (to our knowledge) exists for goniometry with a hyperspectral instrument for measuring a variety of whole rock samples.

Here, we describe WWU's Three-Axis N-sample Automated Goniometer for Evaluating Reflectance (TANAGER). (The acronym TANAGER also has local significance, as the Western Tanager is a brightly colored bird native to Washington state.) TANAGER derives heritage from the WWU Mars Lab's previous planar goniometer (Hoza & Rice, 2019), which allows for automated collection of spectra from multiple bulky samples at varying incidence and emission angles. TANAGER substantially improves upon the planar goniometer design with the capability to collect out-of-plane geometries (i.e., varying azimuth), which is necessary to characterize the full bidirectional reflectance distribution function (BRDF). In partnership with the Seattle-based engineering company First Mode, LLC, we designed and characterized TANAGER to support rapid and comprehensive spectrogoniometric studies of natural rock samples.

2. Performance Requirements

To enable rapid collection of reflectance spectra from multiple rock surface across the full scattering hemisphere – as well as rapid analysis of the spectrophotometric datasets – we defined the following top-level requirements for TANAGER:

1. **Scientific Purpose:** The system shall enable collection of VNIR spectra at a range of geometries relevant to spacecraft measurements.
2. **Sample Type:** The system shall enable measurement of bidirectional reflectance for natural, unprocessed samples.
3. **Time Efficiency:** The system shall enable the following 2 concepts of operations: "Quick Runs" (8 hour time limit), and "Detailed Runs" (168 hour time limit).
4. **Data Visualization:** The system shall provide a means of documenting and visualizing the collected spectra.

5. **Safety:** Use of the system shall not result in damage to people, the goniometer, or other equipment, facilities, or samples.

To meet these requirements, TANAGER's high-level design (Figures 2-3) differs substantially from other spectrogoniometer systems, as we outline in Section 3.

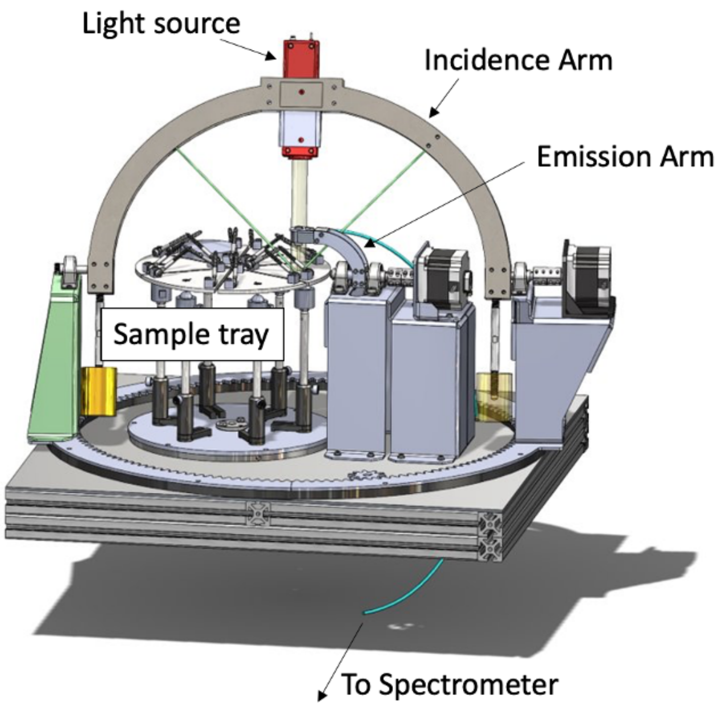

Figure 2. *Schematic of TANAGER with major components labeled. For scale, the dimensions of the baseplate are 80 x 95 cm.*

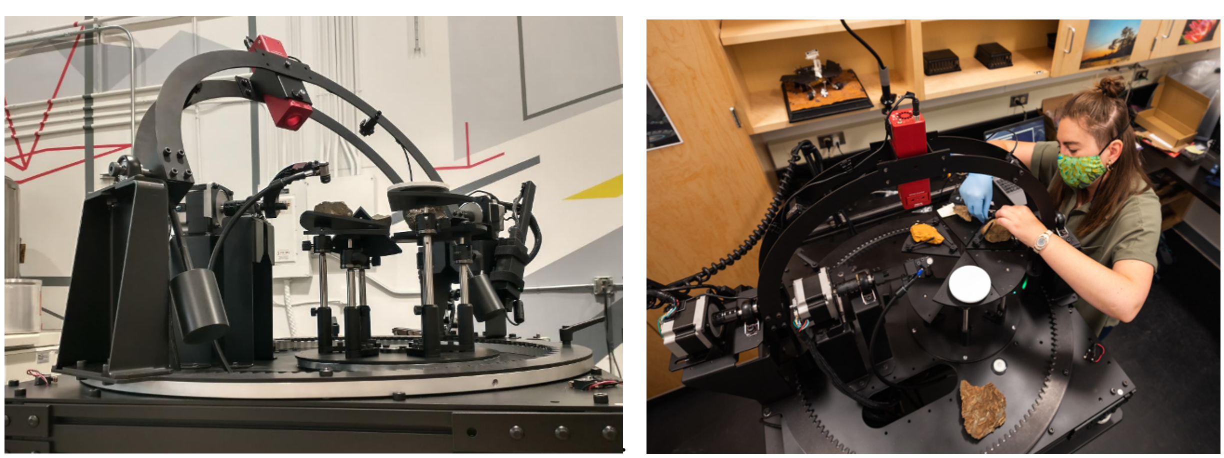

Figure 3. *(left) TANAGER's final assembly at First Mode, LLC (photo by Kathleen Hoza); (right) Samples being positioned on TANAGER's rotating sample tray for analyses in WWU's Mars Lab (photo by Rhys Logan).*

Each top-level requirement yields multiple sub-requirements (Table 1). First Mode, LLC evaluated all requirements except for sub-requirements 1.13, 2.1, 2.2 and 2.4, which were evaluated at WWU upon delivery of TANAGER in Spring 2021 (see Text S1-S5). Every sub-requirement has been met except for the detector head not falling inside the incident light beam for g >= 20° (sub-requirement 1.1). However, we find the small shadow cast at g = 20° to be acceptable, as it is outside the detector pointing (Figure S1). Eight of the sub-requirements were also reevaluated after 300 hours of TANAGER run time (Table S1), which yielded recommendations for long-term operations of the hardware (Table S6).

Table 1: *Summary of the sub-requirements for TANAGER, which derive from the top-level requirements listed in the text. All sub-requirements have been met except for 1.10 (which was met within an acceptable threshold, as discussed in the text).*

Sub-Requirement	Description
1.1 Range	The system shall enable measurements with ● azimuth from 0° to 170° ● emission from -70° to 70° ● incidence from -70° to 70°
1.2 Phase angle	The system shall enable measurements at phase angles from 10° to 140°
1.3 Angular control	The system shall have knowledge and control of detector and light source with 1° steps in all directions
1.5 Pointing accuracy - light source	The center of the illuminated spot shall not deviate from the target point by more than +/- 10% of the illuminated spot diameter
1.6 Pointing accuracy - detector	The center of the detector spot shall not deviate from the target point by more than +/- 10% of the detector spot diameter
1.7 Light bulb operating lifetime	The light bulb shall have an operating lifetime of at least 100 hours
1.8 Target plane indicator	The goniometer shall provide the user with a clear indicator of whether a surface is in the target plane

1.9 Proximity to light source	The detector head and fiber optic shall not come within 5 mm of the light source during normal operations
1.10 No incident light on detector	The detector head shall not be inside the incident light beam for g >= 20°
1.11 Signal drift from heating at small phase angles	At geometries with phase angles below 20°, the standard deviation for repeated measurements taken over the course of 4 minutes shall not be greater than 0.02
1.12 Noise	For both light and dark samples, noise measured against a Savitzky-Golay smoothed spectrum with window size = 19, order = 2 shall not exceed ● +/- .001 in mid-range (500-2400 nm) wavelengths ● +/- .005 for long (2400-2500 nm) and short (450-500 nm) wavelengths
1.13 Polarization artifacts	Polarization artifacts shall not be more than 0.1 for basalt (or a similar sample) at any geometry where azimuth = 180° or 0°
2.1 Detector spot size	The detector spot size on the sample shall have a diameter less than the size of the Spectralon puck at e = 70° (9.1 cm)
2.2 Light spot size	The brightest part of the light spot size shall be 0.5 cm to 3 cm in diameter at i = 0°
2.3 Sample tray repeatability	Each of the 6 sample tray positions shall be repeatable to within +/- 1 mm
2.4 Sample tray vibration	Sample tray movements and vibrations from other actuators shall not disturb the positioning of rounded coarse sand grains in sample cups
2.5 Sample accommodation	The sample tray shall accommodate up to 5 cylindrical samples (9.1 cm diameter, 0 to 5.1 cm height) plus 1 Spectralon puck
2.6 Center-of-sample markings	The sample tray shall have marked center of sample points for each position
2.7 Large sample compatibility	The sample tray shall not interfere with the measurement of spectra for large (>10 cm) samples
2.8 Irregular sample positioning	The sample tray shall enable 5 different wedge-shaped samples plus the Spectralon puck to be positioned each with a surface that is: ● In the target plane to within +/- 1 mm ● Parallel with the target plane to within +/- 5° ● Sample heights may range from 0-5 cm, diameters from 3-9 cm
3.1 Viewing Geometries	Actuators shall be capable of positioning incidence, emission, and azimuth as described in sub-requirement 1.1
3.2 Sample tray rotation speed	Sample tray movements shall occur at an average speed of at least 4° per second
3.3 Viewing geometry adjustment speed	Incidence, emission, and azimuth movements shall occur at an average speed of at least 0.2° per second

3.4 Automatic software startup	Software on the spectrometer computer and raspberry pi shall start automatically
3.5 Legacy software	Unless otherwise noted, software shall provide the same functionalities and experience as existing software
3.6 Iteration across a range	Software shall enable data collection while iterating at a set interval through a range of incidence, emission, and azimuth angles as described in sub-requirement 1.1
3.7 Goniometer visualization	Software shall provide a visualization showing the software's understanding of the current state of the 3D goniometer including incidence angle, emission angle, azimuth angle, and sample tray position
3.8 Communication speed (microcontroller)	Communicating commands to and from the microcontroller shall take no longer than 1 second
3.9 Communication speed (spectrometer computer)	Communicating commands to and from the spectrometer computer shall take no longer than 1 second
3.10 Time limit (limited run)	A limited run of data collection shall take no longer than 8 hours
3.11 Number of samples (limited run)	A limited run of data collection shall characterize 1 sample
3.12 Viewing geometries (limited run)	A limited run of data collection shall include the following geometries: ● For a single plane (az = 0°) measure e, i with 10° resolution ● Outside that plane - 30° azimuthal resolution, 5 geometries at each azimuth ● Leave out reciprocal and rotationally equivalent geometries
3.13 Time limit (detailed run)	A detailed run of data collection shall take no longer than 168 hours
3.14 Number of samples (detailed run)	A detailed run of data collection shall characterize 5 samples
3.15 Viewing geometries (detailed run)	A detailed run of data collection shall include the following geometries: ● 30° azimuthal resolution ● At each azimuth, 10° angular resolution for incidence, emission
3.16 Spectra per sample	At each geometry, a measurement of a single sample shall consist of averaging 200 spectra
3.17 Human operator time	Setting up a run of data collection shall not require more than 60 minutes of time from a human operator
4.1 Data processing/ visualization	Software shall be capable of processing and plotting data sets of up to 5000 spectra
4.2 Feature requests	Additional features may be added
5.1 Light source casing temperature	The temperature of the light source shall not exceed 60° C

5.2 Securability	The sample tray shall be securable
5.3 Position detection	The goniometer incidence, azimuth, and emission positions and the sample tray position shall be detected at the start of operations
5.4 Collision avoidance	Software shall not allow incidence, emission, or azimuth arms to collide with each other

3. Design and Characterization

3.1 Incidence Arm and Light Source

The primary design difference between TANAGER and most existing goniometers is the use of rotating and tilting arcs instead of straight arms, with the addition of cylindrical bronze ~1.5 kg counterbalance weights to provide stability and require less torque from the motors (Figure 4). The TANAGER system enables incidence and emission angles of -70^o to 70^o, and stepper motors allow for automated, repeatable movements to defined geometries sampling the full scattering hemisphere. This range of angles is sufficient to characterize scattering behavior using the Hapke model (e.g., Schmidt and Fernando, 2015).

Using two green laser guides on the incidence arm (Figure 5), we can ensure that the surfaces of bulky samples are positioned precisely in the focal plane. The brightest portion of the illuminated spot size in the focal plane at i = 0^o is 2.7 cm in diameter, and larger at higher incidence angles (but always <9.1 cm, per sub-requirement 2.2; Table 1). Because the illuminated spot size is not actively controlled, it is possible to measure slightly different portions of the sample surface at different incidence angles, especially with high emission angles where the detector spot (which is similarly not actively controlled) can be larger than the illuminated spot. Users should take this into consideration for high phase angle measurements of non-uniform samples.

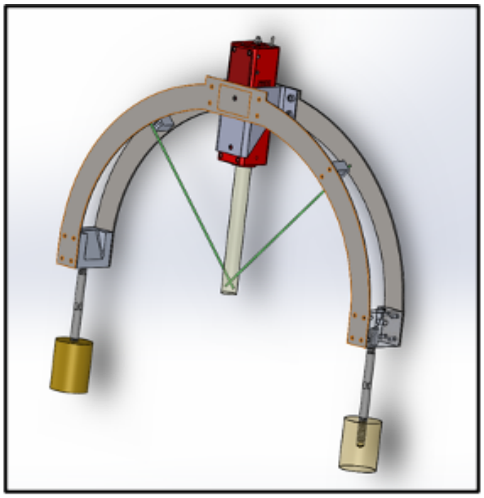

Figure 4. *Schematic of TANAGER's incidence arm. The diameter of the arc is 67 cm. Illumination is provided by a Thorlabs VNIR light source, and two bronze weights provide counterbalance. Two green laser guides intersect at the focal plane.*

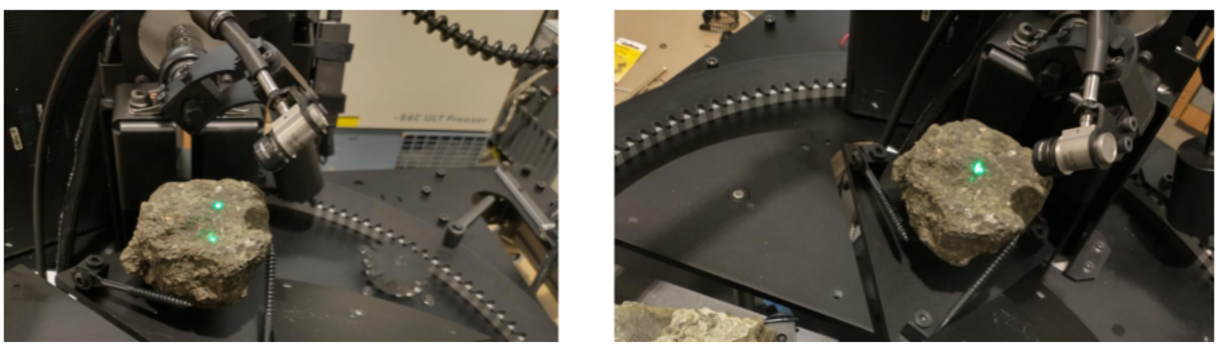

Figure 5. *Green laser guides indicate when the sample is out of the focal plane (left) and within the focal plane (right, when two dots become one).*

The apex of the incidence arm supports a Thorlabs SLS201L light source with integrated cooling system and peak output near 1000 nm (Figure 6). This commercial light was selected for its relatively long bulb lifetime, sufficient power output across the 400-2500 nm wavelength range, and minimal heating. We characterized heating on color standards and geologic targets in the focal plane (Text S1) and found the temperature increases to be minimal: Spectralon®, which heated negligibly (0.4°C), and other targets' temperatures increased by 2-4°C over typical exposure durations (~2 minutes of direct illumination during nominal TANAGER operations) (Figure S2). We also characterized the effects of incident light heating on adsorbed water by monitoring spectral changes to powdered anhydrite ($CaSO_4$) over time (Text S2). During 30 minute periods of exposure, we observed no changes to the hydration absorptions attributed to adsorbed water on grain surfaces (Figures S2-S4), which gives us confidence that the sample heating is too minimal to drive adsorbed water off mineral grains or otherwise dehydrate samples.

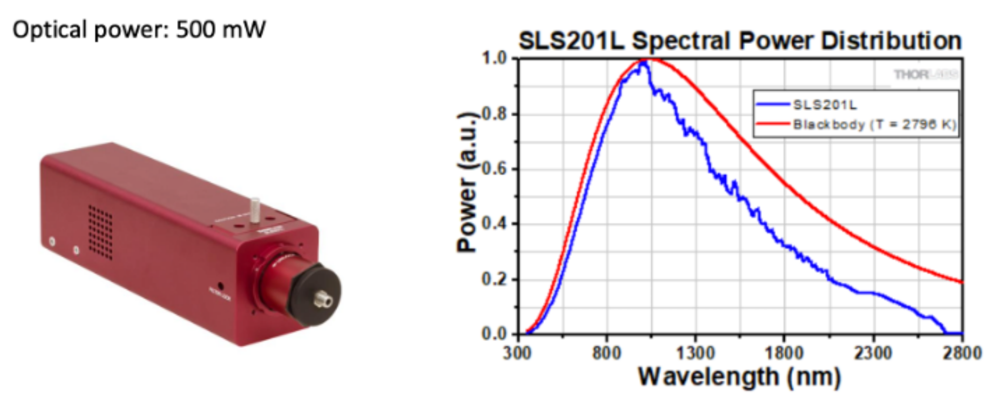

Figure 6. *Thorlabs VNIR light source (left) with power distribution curve for a blackbody and as measured (right).*

3.2 Emission Arm

TANAGER interfaces with a Malvern PanAnalytical ASD FieldSpec4 Hi-Res reflectance spectrometer (hereafter, "FieldSpec"; Section 3.5), and its emission arm is designed to accommodate the fiber optic cable attached to the spectrometer (the reflectance probe). Like the incidence arm, the emission arm uses stepper motors for precise, repeatable positioning of emission angles from -70º to 70º. The design of the arm is an arc (Figure 7) with a collimating lens that reduces the detector spot size at the focal point. Reflected light entering the collimator is directed to the fiber optic cable via an angled mirror at the end of the emission arm. We characterized how the detector spot size changes with emission angle (Text S3) and found a minimum of 1.6 cm at e = 0° and a maximum of 3.5 cm at e = 70° (Table 2). At small incidence angles, this means that the detector spot falls entirely within the illuminated portion of the sample for emission angles < 50°.

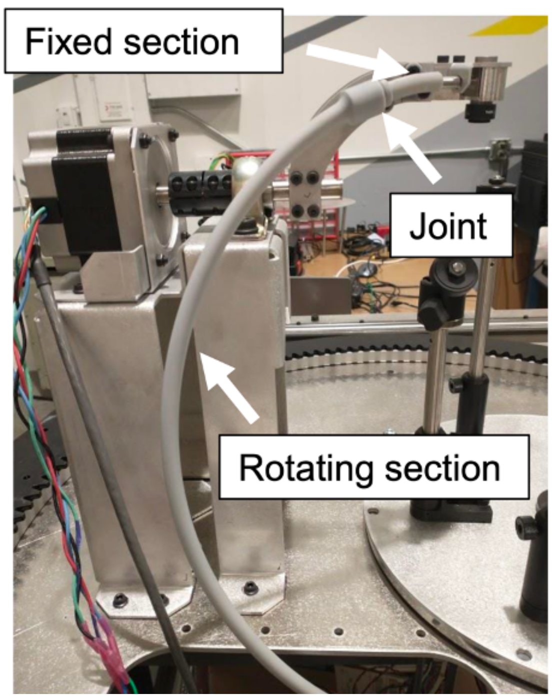

Figure 7: *Components of the emission arm's tubing, which guides the position of the FieldSpec's fiber optic cable and maintains a wide arc at all geometries.*

Table 2: *Detector spot size ranges measured for different emission angles (see Text S1).*

Emission angle (°)	Measured Spot Size Range (cm)
0	1.6-2.0
15	1.8-2.6
30	1.8-2.2
50	2.4-2.8
70	2.8-3.5

The emission arm design ensures that the spectrometer's fiber optic cable (the reflectance probe) does not bend in any geometry. A guide tube keeps the fiber in a repeatable position from one measurement to the next, which consists of a short, fixed portion close to the detector tip and a longer, rotating portion farther back (Figure 7). This tubing allows for the fiber optic to be easily removed and replaced when the FieldSpec needs to be detached from TANAGER (e.g., when used with a Malvern Panalytical Contact Probe or Small Diameter Probe). To prevent bending of the fiber optic, the system is designed to maintain a 35 cm diameter of curvature.

3.3 Azimuth Turntable

The incidence arm is mounted to a geared turntable which controls azimuth angle between 0º and 180º (Figure 8). The large gear ratio reduces the necessary torque and increases angular accuracy. The system includes a homing routine with stops installed onto the baseplate. One challenge in the azimuth design is the need to manage cables for the light source, incidence motor, and incidence encoder as azimuth changes. The solution in TANAGER's initial design used the combination of slider, coiled cable, and spring-loaded arm to enable consistent motion across the azimuth range (Figure 9). However, upon extensive use in WWU's Mars Lab, we found that the slider's and spring arm's motions were finicky, so we attached the coiled cable to a fixed lab surface with ample clearance instead (Figure 10).

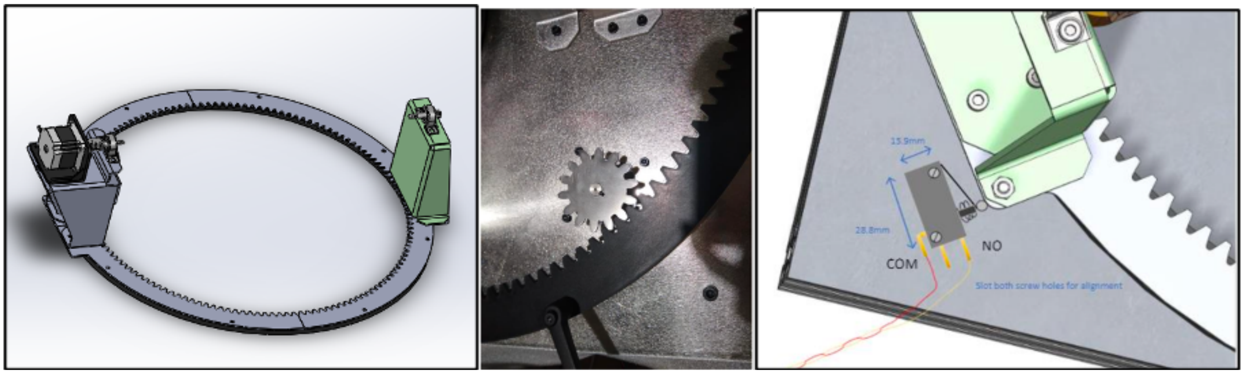

Figure 8. *Left: Schematic of the azimuth turntable mounted with the attachments and stepper motor for the incidence arm. Middle: Detail of gears for the azimuth turntable. Right: Schematic of the homing mechanism on the azimuth baseplate.*

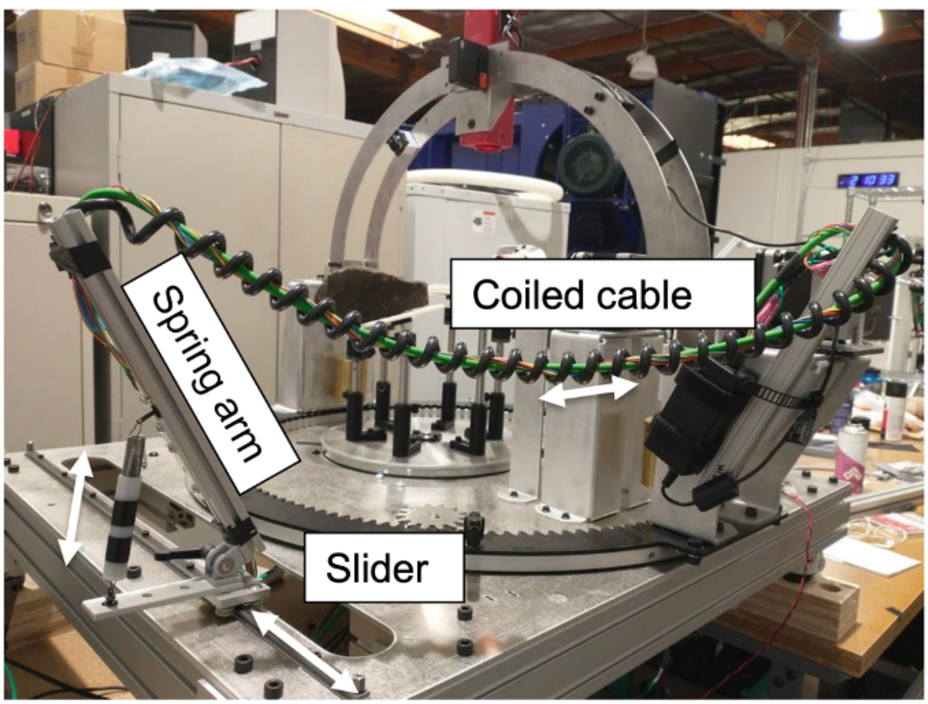

Figure 9. *Initial cable management solution for the full range of azimuths (0 º to 180º).*

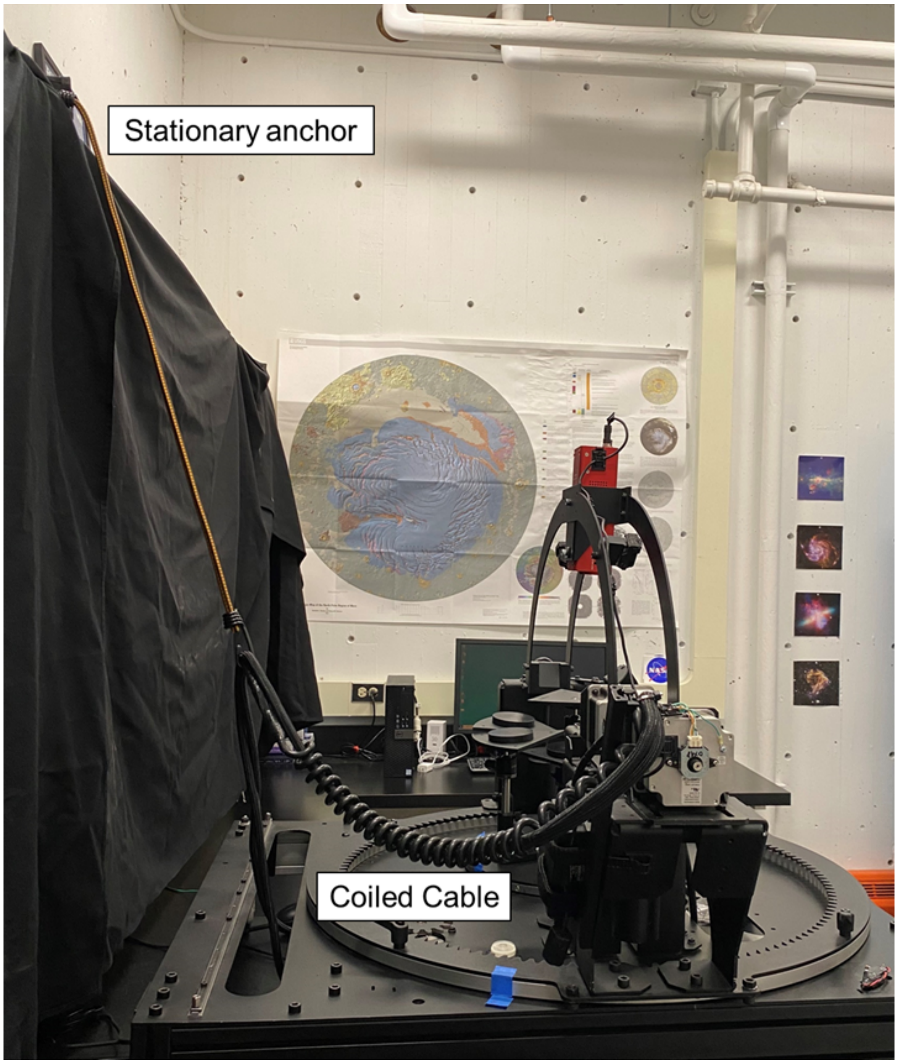

Figure 10. *Final cable management solution for the full range of azimuths (0º to 180º).*

3.3 Sample Trays

The goniometer design includes two stages for positioning samples within the focal plane. Both are motorized and can rotate up to five samples in and out of the field of view with a Spectralon® white reference correction at each geometry. The first is a single, height-adjustable surface designed for multiple samples of the same height (e.g., particulates in sample cups) or for a single, bulky hand sample (Figure 11). For use with this stage, we designed sample cups at the same height as the white reference and risers for positioning Scanning Electron Microscope (SEM) mounted samples.

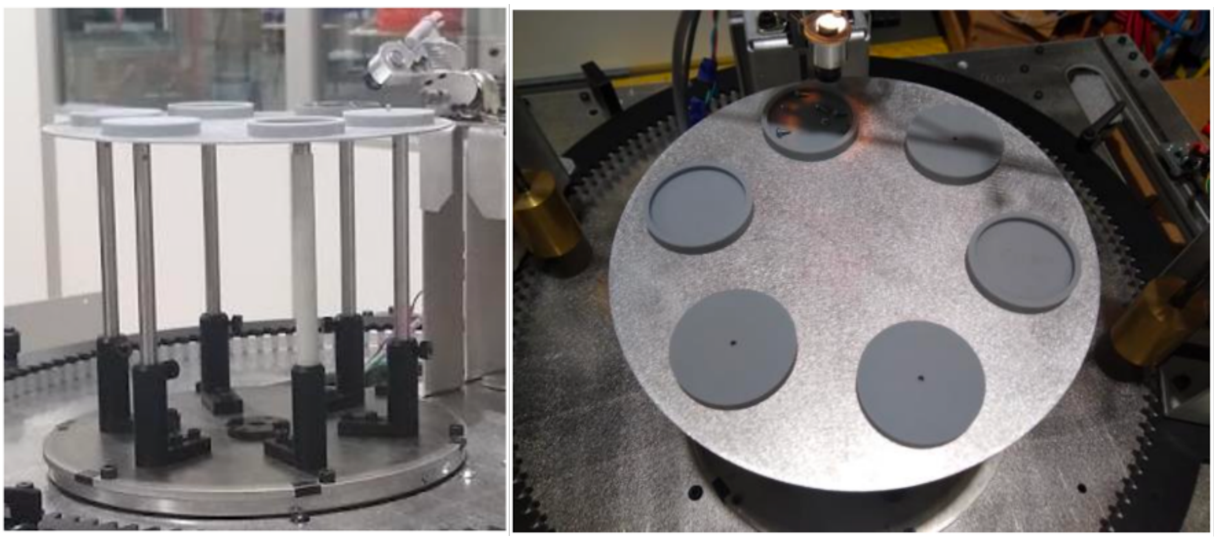

Figure 11. *Left: Single-height, rotating sample stage. Right: Custom sample cups and risers for SEM mounts designed with the same height as the Spectralon® white reference puck.*

The other stage consists of six pie-slice-shaped sample supports, each of which can be moved independently (height and tilt) to accommodate a variety of bulky samples (Figure 12). Many degrees of freedom are required for positioning a near-flat portion of each sample into the focal plane. Adjustable screws can be added/removed to keep samples in place, and multiple sample supports can be used to support a single, awkward sample (Figure 12 right). In characterizations of sample tray motion during TANAGER operations (Text S4), we found that vibration was undetectable during incidence and emission arm motions, and minimal during azimuth and tray motions (Figure S5). TANAGER's movements are highly unlikely to change the positions of samples on the tray or shift loose material within sample cups (Figure S6).

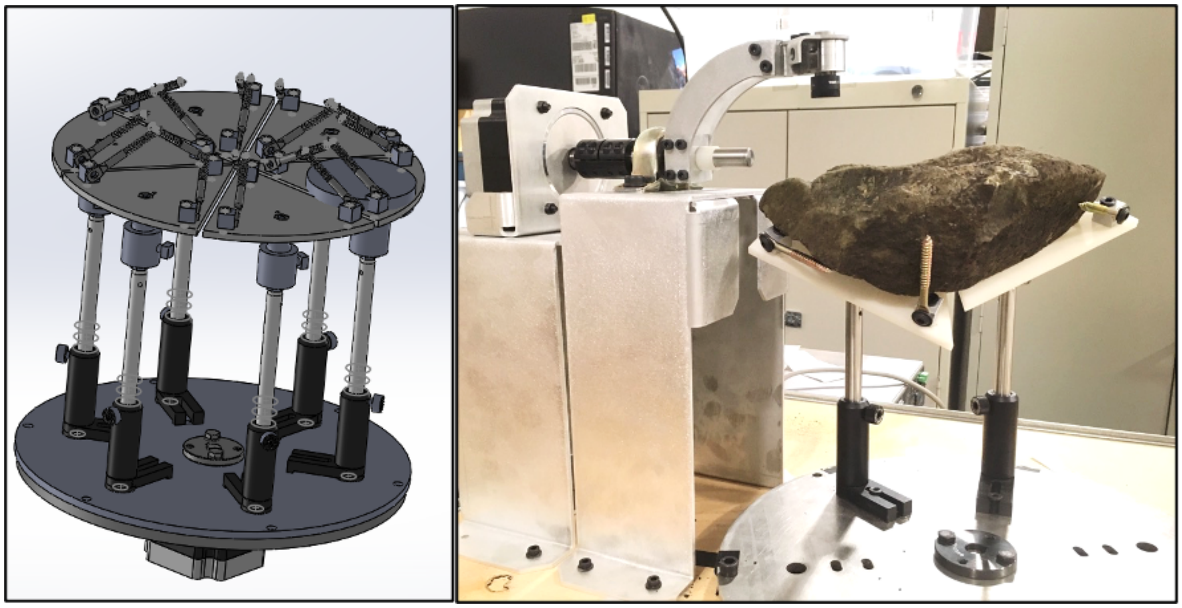

Figure 12. *Left: Schematic of the multi-height, rotating sample stage. Six independently-adjustable, pie-slice-shaped supports allow for the positioning of a variety of samples. Right: Example of a bulky, awkward sample positioned with a horizontal surface in the focal plane using two supports and stabilizer screws.*

3.4 Paint

Before delivery of TANAGER, all components were coated with a matte black paint to minimize stray light reflections from the metallic surfaces. We collected VNIR spectra for a range of different black paint options (LabIR Paints, Rustoleum, Fusion, black30), and all exhibited similar spectral shapes and low albedos throughout the 400-2500 nm range. Specular properties for all materials were also similar. Thus, we looked to mechanical adhesion and wear and selected LabIR Paints (https://paints.labir.cz/en/) because it performed best in mechanical tests. We applied the black paint to TANAGER via aerosol (Figure 3).

3.5 Spectrometer Interface

Sample spectra (averages of 200 for each) are measured relative to a Spectralon® white reference target at each geometry and corrected for minor (<2%) irregularities in absolute reflectance and for small offsets at 1000 and 1830 nm where detector changeovers occur (e.g., Cloutis et al., 2008). The ideal white reference material would be a perfectly Lambertian reflector (scattering incident light equally at all viewing geometries); in practice, however, such a material does not exist, but the geometry-dependent reflectance properties of Spectralon® have been well-documented (e.g., Shaw et al., 2016). We have incorporated the published Spectralon® corrections for high phase angles from Bhandari et al. (2012), using a linear interpolation when needed, into the analysis software (Section 2.9).

Other challenges to the spectrometer interface occur at high phase angles, where the emergence of artifacts near 1100 and 1310 nm in spectra from FieldSpec and similar spectrometers have been documented (e.g., Buz et al., 2019) and shown to originate from polarization of the sample and probe (Levesque & Dissanska, 2016). These polarization artifacts are challenging to correct, but fortunately, their wavelength positions do not interfere with the locations of the prominent spectral features and absorptions in rock-forming minerals and their alteration products. We quantified the strength of these artifacts for our prototype planar goniometer (Hoza & Rice, 2019), for a variety of materials at a range of phase angles, and found that they were consistently negligible (<1%) at phase angles between $g = -20^{o}$ and $g = 40^{o}$. Therefore, we designed an option to omit the region 1050-1350 nm from TANAGER's high phase angle analyses, as done by Buz et al. (2019). However, we have rarely needed this option in practice, as TANAGER's spectra rarely exhibit polarization artifacts (and, when they do appear, they are < 2%; Text S5; Figure S7).

3.6 Automation and Control Software

Automation is a critical design component of TANAGER. Our previous studies verified the need for an automated system: using our prototype planar goniometer (Hoza & Rice, 2019) with a simple control software, we found that our rate of data collection increased by almost an order of magnitude. When manually positioning targets and the goniometer arms, acquiring measurements at 10 viewing geometries with Spectralon® white reference correction took roughly 90 minutes for a single sample and required an attendant in the lab to adjust the goniometer and perform the white reference calibration every few minutes. However, with automation, we acquired spectra of five samples with white reference corrections at 10 viewing geometries each in under 60 minutes total, including time for data processing and plotting, with minimal need for supervision by a lab attendant (Hoza & Rice, 2019). For more detailed analyses requiring high angular resolution (~100 geometries), automation reduced the total acquisition time per sample from ~15 to ~2 hours.

For TANAGER, a total of four stepper motors drive the incidence, emission, azimuth, and sample tray components, as described above. First Mode, LLC designed custom software for TANAGER in open source packages called "tanager-feeder" (Hoza, 2023). The software operates three computers all connected to a local spectroscopy lab network (Figure 13):

1. *Control computer.* This is where the user gives input. Software running on this computer includes a Python Graphical User Interface (GUI) that allows the user to input all parameters relating to sample configuration, spectrometer configuration, and desired

viewing geometries. This GUI also displays information about the current state of the system (Figure 14) and includes a log of all actions taken during the current session.

2. *Spectrometer computer.* This computer is controlled via command files generated by the control computer and dropped into a shared folder on the local network. Following instructions in these command files, it runs GUI automation software that operates the proprietary spectrometer control software (RS3) and spectral processing software (ViewSpec Pro). This enables the instrument to be optimized and for a white reference taken at each viewing geometry. After each run of data collection, this spectral processing software is used to apply a splice correction to remove artifacts generated at the positions where spectrometer detectors overlap.

3. *Raspberry Pi.* This computer is also controlled via command files generated by the control computer and dropped into a shared folder on the local network. Following instructions in these command files, it operates the motors driving the goniometer arms and sample tray. The software is designed with safety in mind; for example, it keeps the emission and incidence arms out of harm's way while other parts are rotating. The control system also notices if motorized parts are not making progress and stops and alerts the user via the control computer.

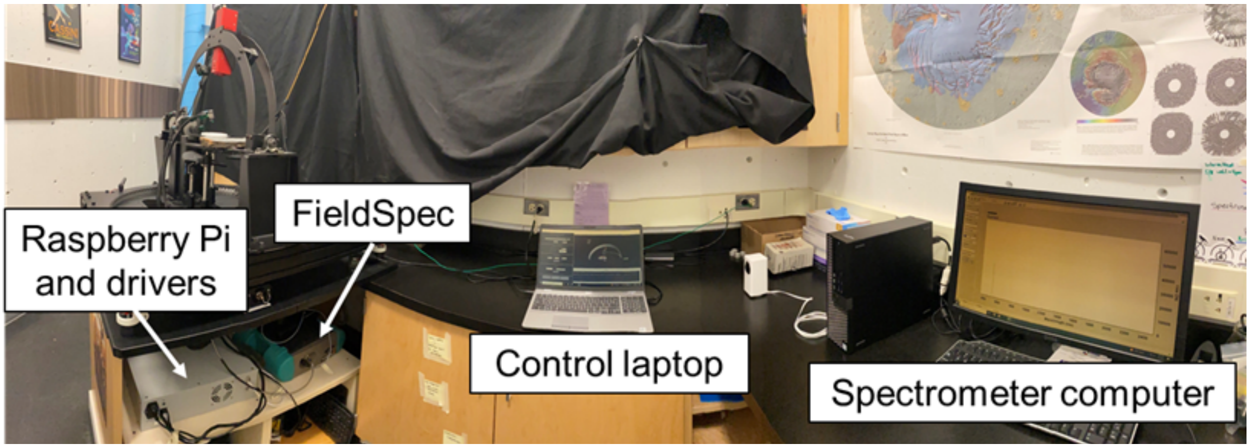

Figure 13. Panoramic photo of the lab containing TANAGER (upper left) showing the relative placements of the FieldSpec, Raspberry Pi, control laptop, and spectrometer computer. Blackout curtains are hung behind TANAGER in order to minimize stray light.

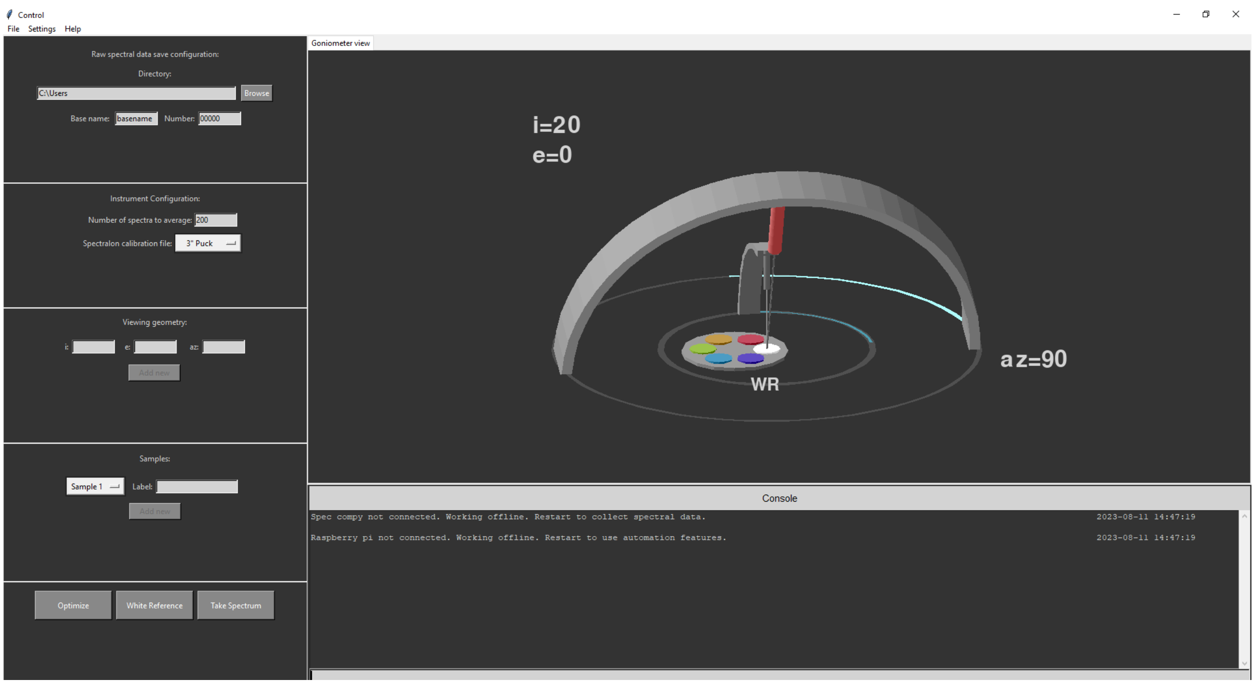

Figure 14. *Screenshot of "tanager-feeder" control software GUI with settings on the left, visualization of current goniometer and sample stage configuration on the upper right, and command line interface at lower right.*

3.7 Analysis Software

In addition to operating the goniometer and spectrometer, the "tanager-feeder" software includes a suite of tools that can be used to view and analyze spectrophotometric data. In the simplest case, a selected set of spectra are plotted with wavelength on the x-axis in nanometers and reflectance (relative or absolute) on the y-axis (Figure 15a). Additional analytical capabilities include normalizing spectra to 1.0 at a given wavelength (Figure 15b); calculating spectral slope (defined as the change in relative reflectance divided by the change in wavelength in nm; Figure 16); calculating band centers and depths of features between user-defined shoulder wavelength positions (as defined by Clark, 1999); calculating average reflectance for all values between a give wavelength range; adding offset values to spectra for clarity (Figure 17); and excluding wavelength regions with known artifacts (Figure 18).

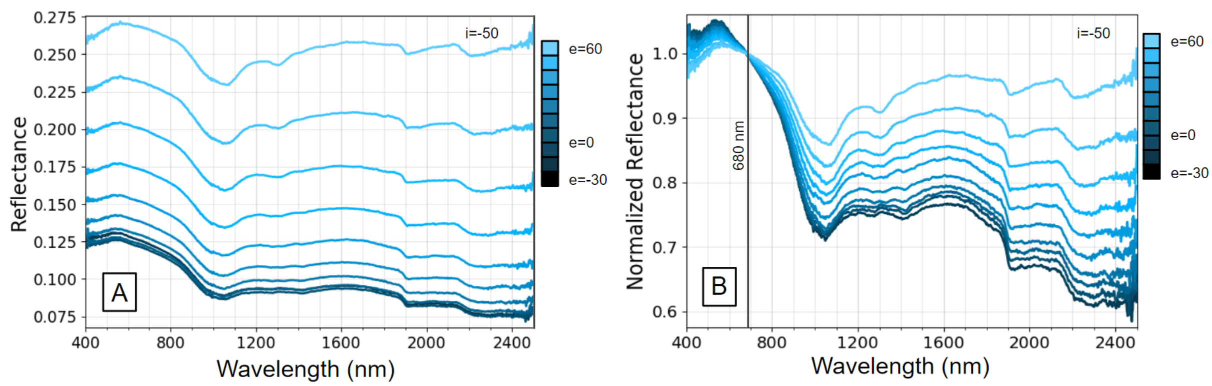

Figure 15: *Example of spectra before (a) and after (b) normalization to 1.0 at wavelength 680 nm.*

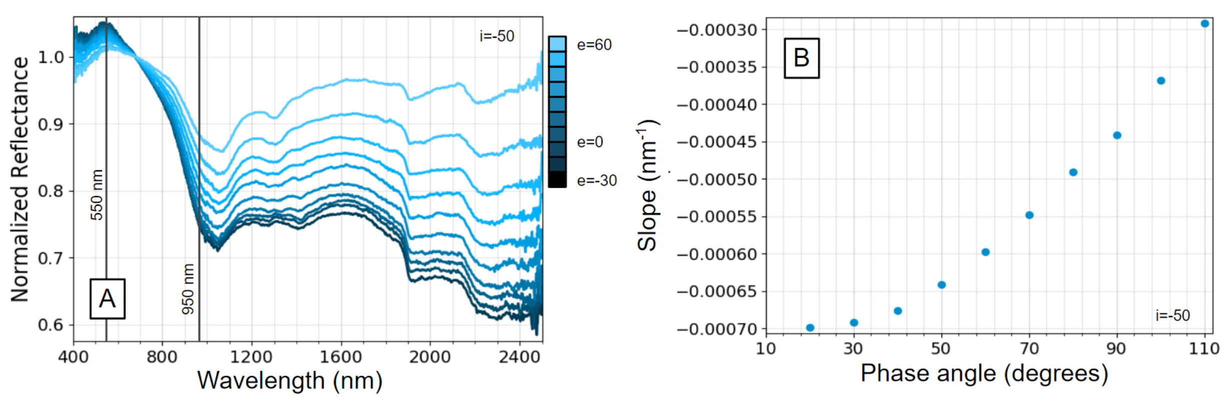

Figure 16: *Spectral slopes are calculated from a range of wavelengths identified for spectra of interest (a) and can be plotted as a function of phase angle g (b). In this case, slopes are calculated from 550-950 nm and are shown to become less negative as phase angle increases.*

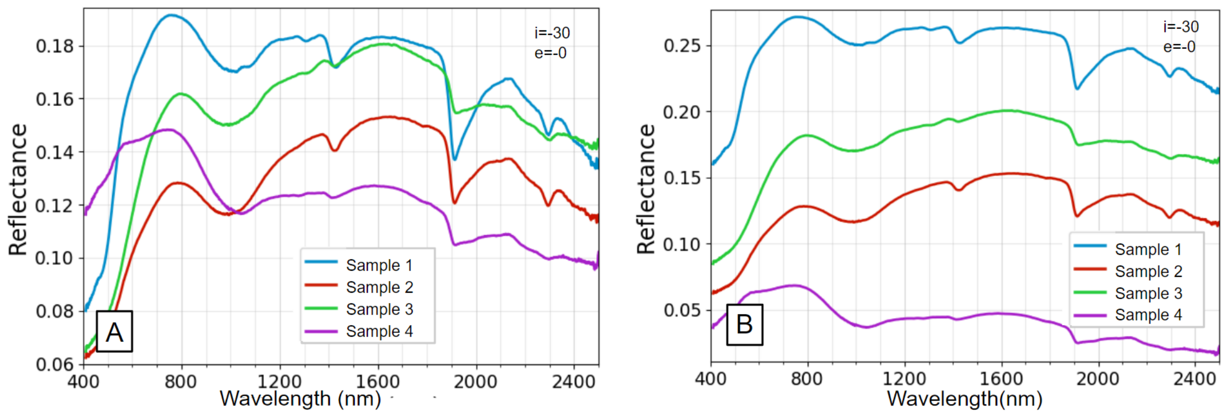

Figure 17: *Overlapping spectra (a) can be hard to interpret, but adding offsets to samples can add clarity (b).*

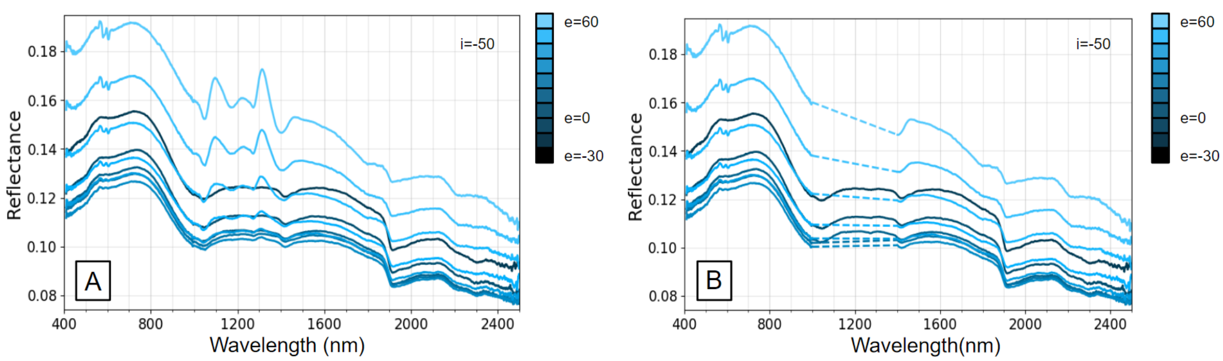

Figure 18: *Polarization artifacts can appear within wavelengths 1000-1400 nm at high phase angles (a), so these regions can be omitted from our results for given geometries and replaced with dashed lines (b). Spectra shown are from the WWU Mars Lab's planar goniometer (Hoza & Rice, 2019); in practice, TANAGER spectra rarely exhibit polarization artifacts (Text S5; Figure S7).*

When interpreting spectra taken at a wide range of geometries, alternative visualization techniques can be beneficial for displaying some photometric behaviors. For example, to show the shapes of scattering lobes for measurements in a single plane (fixed azimuth), two-dimensional hemispherical plots can be much more effective than the original spectra (Figure

19). Our software also allows fixed azimuth data to be displayed with a heatmap; in these plots, emission angle is on the x-axis, incidence angle on the y-axis, and a user-defined parameter (such as reflectance at a given wavelength, band depth of a specific features, etc.) is represented by a color scale (Figure 20). For three-dimensional datasets (including variations in azimuth angle), the software enables visualizations of spectrophotometric behaviors as scattering lobes and/or heatmaps (Figure 21).

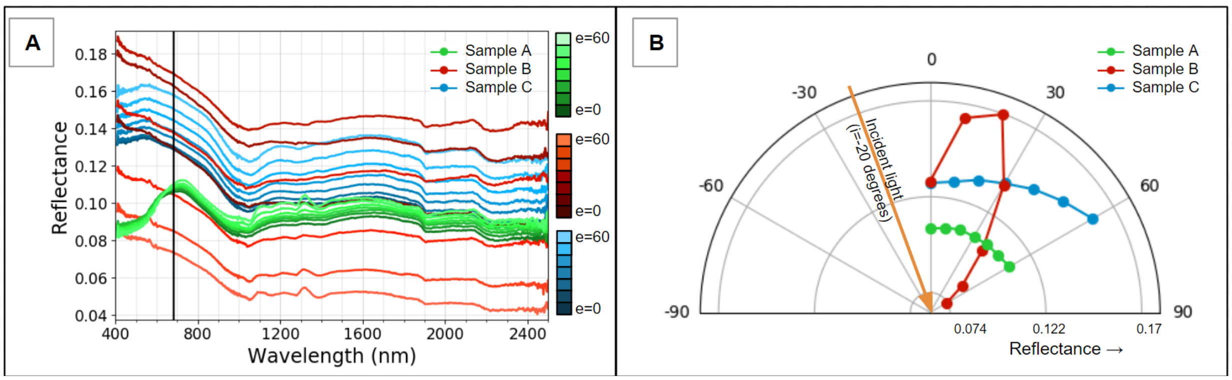

Figure 19: *Examples of two-dimensional hemispherical plots: (a) Reflectance is measured for three samples at an incidence angle of -20 degrees and emission angles varying from 0 degrees to 60 degrees. (b) Reflectance values at 680 nm are plotted on a hemispherical plot with reflectance on the radial axis and emission angle varying with theta. Spectra shown are of uncoated (blue, green) and silica-coated (red) basalt surfaces (Hoza, 2019).*

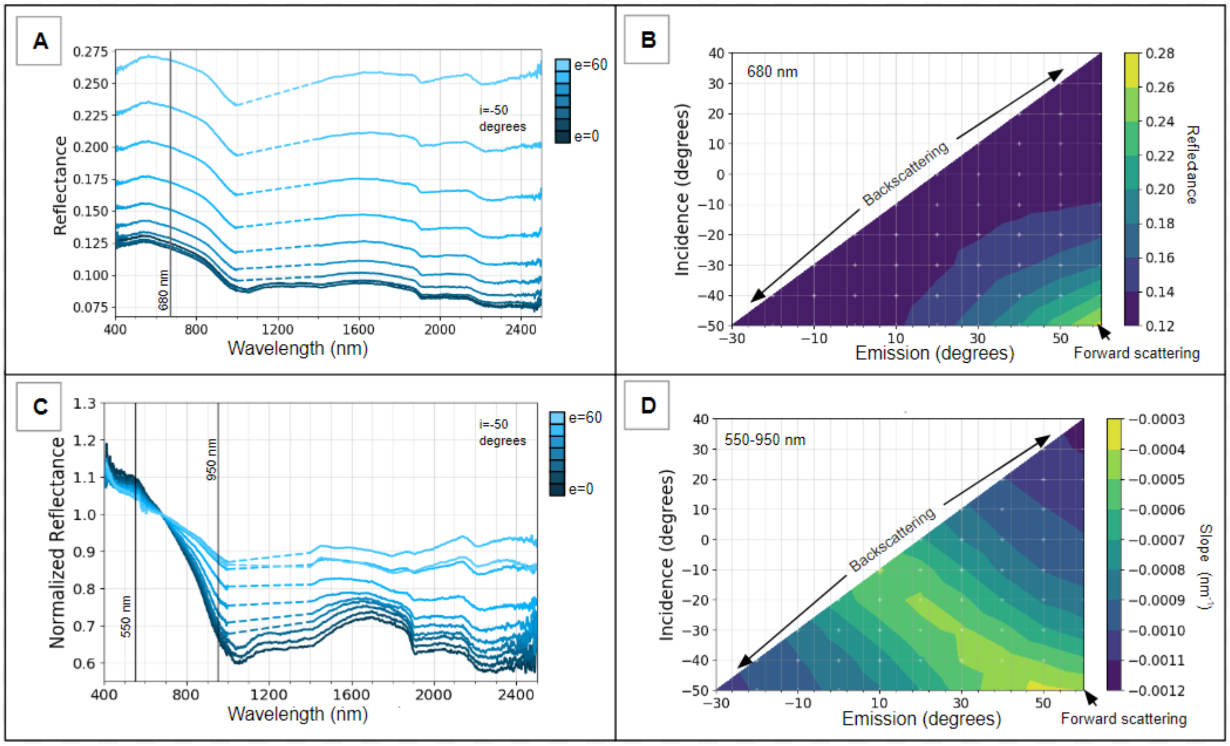

Figure 20: *Examples of two dimensional "heat map" plots: (a) Reflectance is measured at 6all viewing geometries for a given sample (incidence = -50º shown here). (b) Reflectance at 680 nm is plotted as a heat map in incidence, emission space with a color scale representing a range of reflectance. (c) For a different sample, slope from 550-950 nm is measured for normalized spectra at all viewing geometries (incidence = -50º displayed here). (d) Slope is then plotted on a heat map over incidence, emission space with the color scale corresponding to different slopes.*

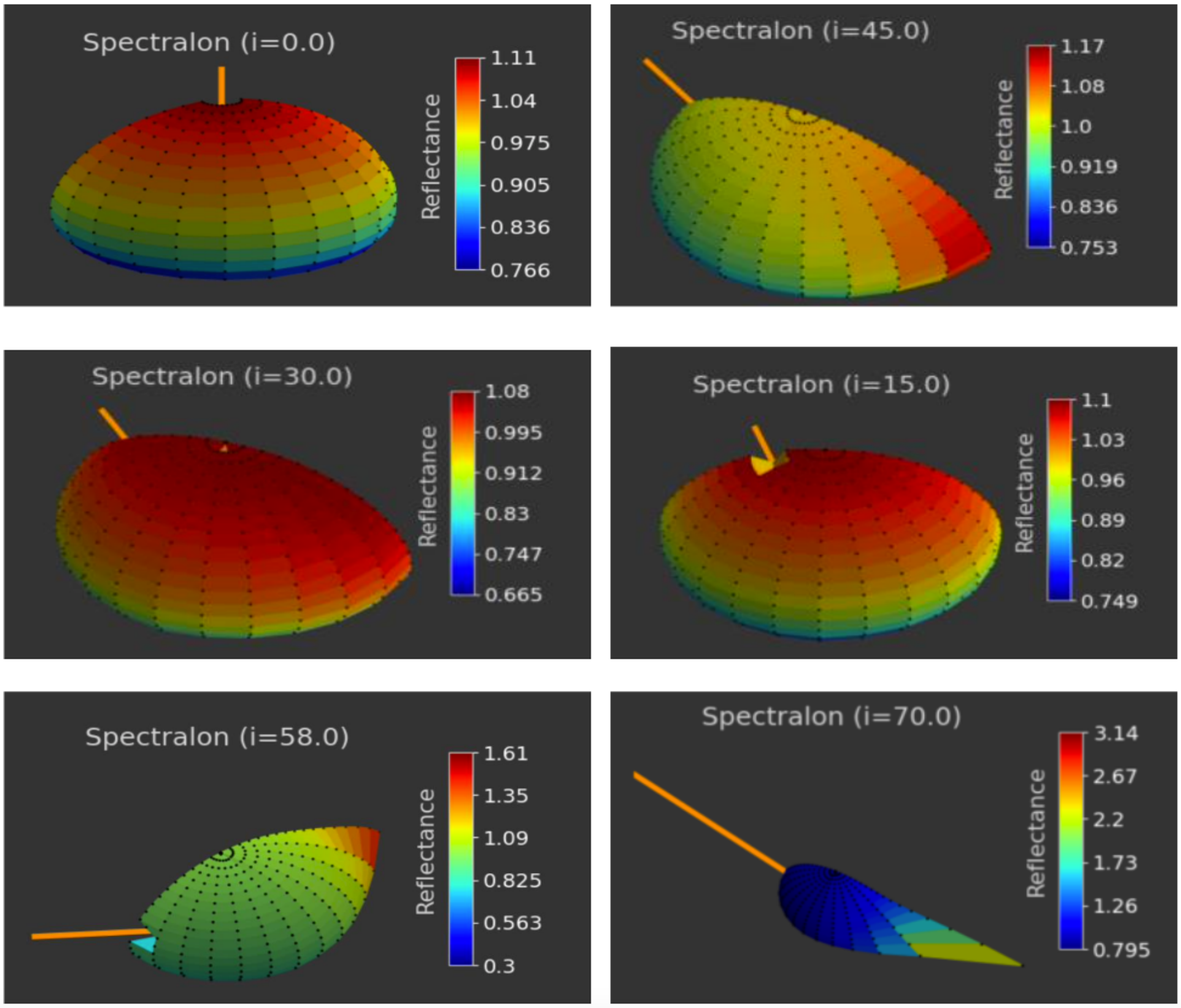

Figure 21: *Examples of three-dimensional hemispherical plots of scattering patterns for the Spectralon® white reference (which is non-Lambertian above i= 45°), for reflectance values at 680 nm.*

3.8 Operational Procedures

Approximately one hour of human operation time is required before TANAGER data collection can be initiated. A number of startup procedures are required to place and secure samples, perform safety checks, input run parameters, and generally ensure that data are collected safely and effectively. Below, we provide a high-level description of human-operator startup tasks for TANAGER data collection in "automatic mode":

1. *FieldSpec warmup:* Turn on the FieldSpec spectrometer to allow it to warm up for 60 minutes, as recommended by the manufacturer (ASD Inc., 2017).
2. *Sample positioning (initial):* While the FieldSpec is warming up, perform the initial sample placements on the sample stage, level targets using a bubble level, and adjust the targets into the measurement plane with the indicator lasers (Figure 5). For larger, natural, or irregular samples, this may require significant manipulation of the sample tray stage and/or securing the sample with supports and stabilizer screws (Figure 12). Finally, test for collisions by manually moving the emission arm to +/- 50° (the steepest emission angle during sample tray rotation), rotating the sample tray 360°, and readjusting sample placement as necessary.
3. *Software setup:* After initial sample placement, turn on the Raspberry Pi, control computer, and spectrometer computer. In the user interface on the control laptop, configure the control computer interface to match the physical TANAGER set up, set the number of spectra to be collected, select the correct white reference calibration file, enter the desired geometries, and name the samples.
4. *Sample positioning (secondary):* With Raspberry Pi on and the stepper motors engaged, recheck the sample placement, leveling, height, and collision risk for each sample and make final adjustments as necessary.
5. *Data collection:* During data collection, light sources unrelated to data collection (e.g. overhead lights and unnecessary computer monitors) should be turned off. A human operator may either remain in the lab (e.g. for a short run of 30 minutes) or leave the lab for the duration of the run (e.g. for multi-day runs) in order to

eliminate stray light from outside the lab. Western Mars Lab uses an infrared webcam to monitor the control computer software and TANAGER hardware for run completion or unexpected errors when the human operator is not in the lab.

4. Data Validation

4.1 Cross-Calibration

We validated TANAGER's data quality by reproducing measurements of calibration target ("caltarget") materials from Buz et al. (2019). The caltargets are a set of exceptionally well characterized color standards and are the reference targets for the Mastcam-Z instrument on the NASA Mars 2020 *Perseverance* rover (Kinch et al., 2020). These caltargets have also been used in the calibration of Mastcam-Z's legacy instruments: Mastcam on the NASA Mars Science Laboratory *Curiosity* rover (Bell et al., 2017) and Pancam on the NASA Mars Exploration Rovers (Bell et al., 2006). The eight caltargets include AluWhite from Avian Technologies LLC; and Cyan, Green, Red, Yellow, Gray33, Gray70, and Black from Lucidion Inc.. Spectra from each target were collected at same geometries of Buz et al. (2019) and evaluated at subset of phase angles: backscattering geometry (i = 30°, e = 45°, az = 0°, g = 15°), standard geometry (i = 0°, e = 30°, az = 0°, g = 30°), specular geometry (i = -30°, e = 30°, az = 0°, g = 60°), forward scattering geometry (i= -45°, e = 30°, az = 0°, g = 75°), and very forward scattering geometry (i = -70°, e = 58°, az = 0°, g = 128°). Relative root mean square error (RMSE, defined in Text S3) was calculated to compare datasets. We consider a relative RMSE of 5% or less to be an acceptable threshold of error (as is the case in the radiometric calibration of flight hardware such as Mastcam-Z; Hayes et al., 2021).

Spectra from TANAGER agree with those from Buz et al. (2019) to within 0.05 reflectance units for the color and black standards, and to within 0.01 for the grayscale standards, in all geometries except for the highest phase angles (Figures 22-23 and Figures S8-S9). Wavelengths near 1100 nm and 1300 nm typically have large residuals (e.g., Figure 23 gray), which we attribute to known polarization artifacts that are prominent in the data from Buz et al. but nearly absent in TANAGER spectra (see Text S5). We also observe structure in the residuals near 1900 nm (e.g., Figure 22), where there is an H_2O absorption; Buz et al. (2019) note variations in this band strength in their spectra which they attribute to water in the instrument path length, and they recommend caution when interpreting small fluctuations in this region.

We observe the same general scattering behaviors for all targets as those reported by Buz et al. (2019): the brighter samples (light gray, red, cyan and yellow) are quasi-isotropic, the AluWhite sample is weakly backward scattering, and the darker samples (black, dark gray and green) are strongly forward-scattering. TANAGER spectra of the brighter samples suggest they are more isotropic than demonstrated by Buz et al. (2019) (i.e., TANAGER spectra show less variation in reflectance at high phase angles; Figure 22, Figure S8). The two highly forward-scattering geometries ($i = 30^{\circ}$ and $e = -58^{\circ}$, -70°) show reversed behavior in TANAGER spectra compared to Buz et al. (2019); however, the TANAGER spectra are more consistent with the known scattering behaviors for these targets (e.g., the $e = -70^{\circ}$ spectrum is higher reflectance than the $e = -58^{\circ}$ spectrum for strongly forward-scattering targets; Figure 23, Figure S9). Therefore, the discrepancies between the two labs' datasets may indicate improvements in TANAGER spectra over the previously-published versions.

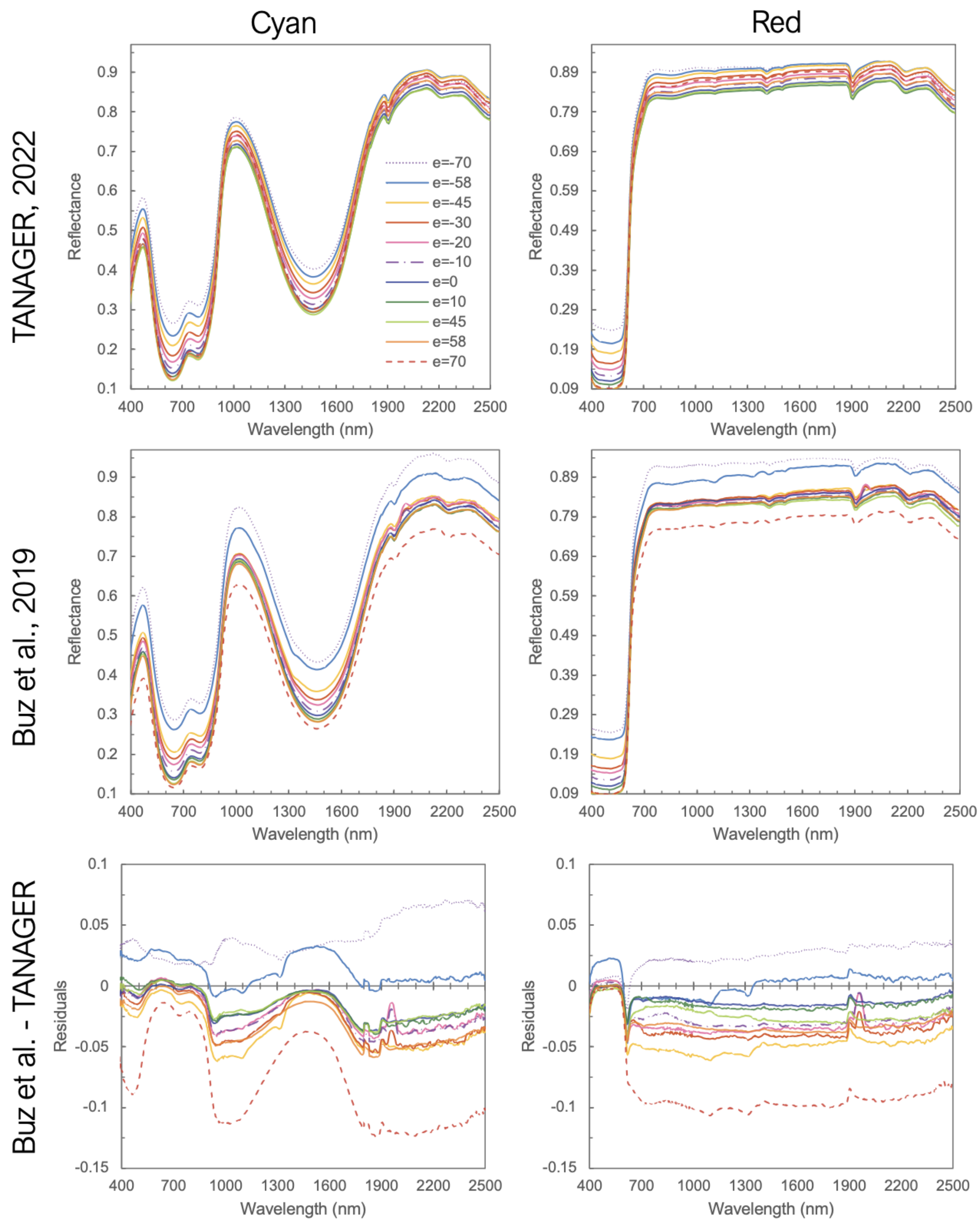

Figure 22: *Spectra of the cyan and red Mastcam-Z caltarget witness samples at multiple viewing geometries from TANAGER (top) compared to Buz et al. (2019) (middle), with residuals (bottom). All measurements were acquired at i = 30º and az = 0º.*

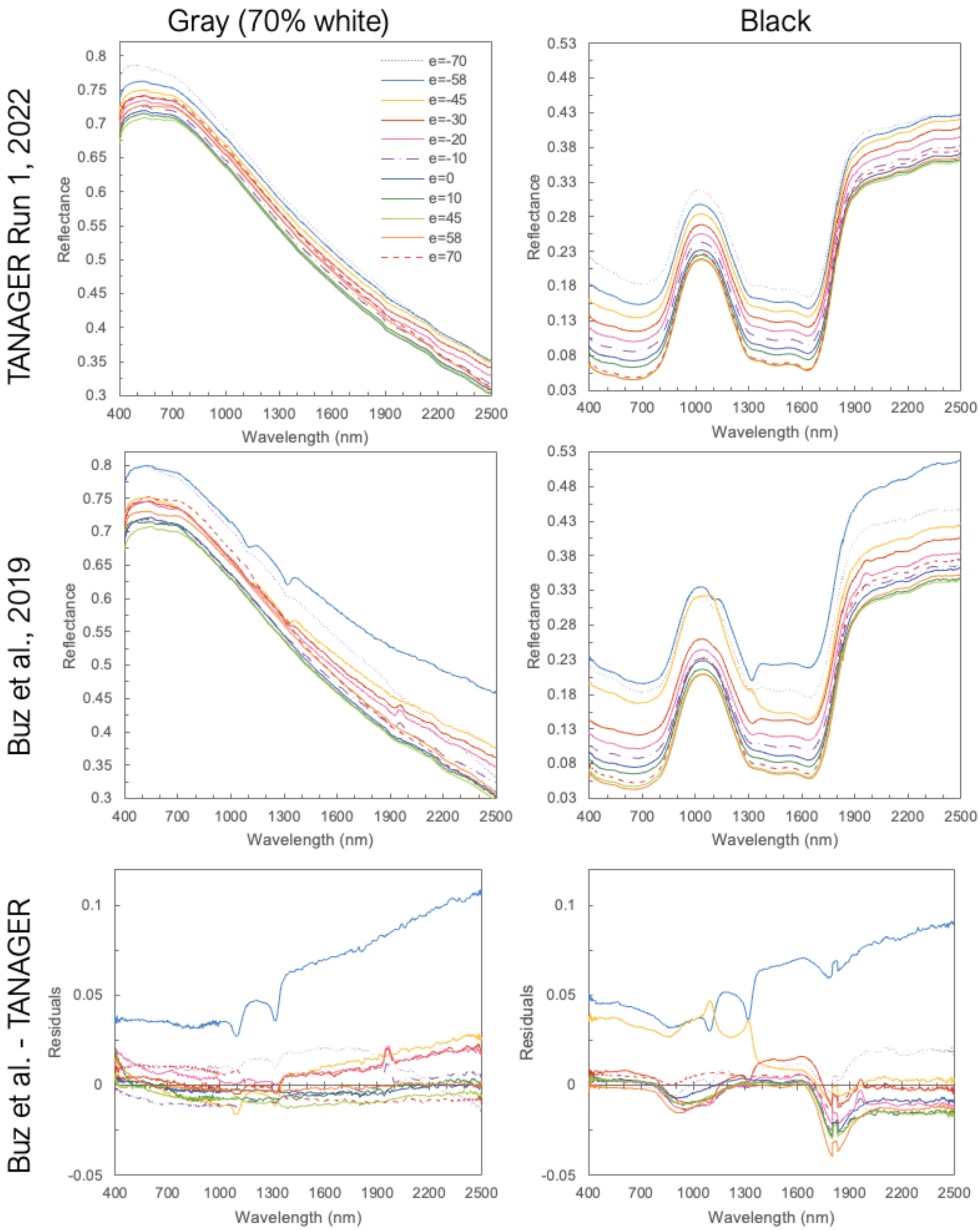

Figure 23: *Spectra of the light gray (70% white) and black Mastcam-Z caltarget witness samples at multiple viewing geometries from TANAGER (top) compared to Buz et al. (2019) (middle), with residuals (bottom). All measurements were acquired at i = 30º and az = 0º.*

To minimize differences in absolute reflectance and focus on differences in spectral shape, we also normalized spectra to 1.0 at 754 nm and calculated relative RMSE at a representative range of geometries. The normalized spectra (Figure 24) have only minor differences in spectral shape and slope (except for the light gray target at $g = 128^{o}$). Relative RMSE values (Table 3) are less than 5% with two exceptions: (1) the black target and (2) highly forward-scattering geometries. We attribute the black target's high relative RMSE to its dark albedo and low signal-to-noise, so we do not find these values concerning, but recommend caution when interpreting subtle spectral shapes in TANAGER spectra of dark materials.

The high relative RMSE values for the very forward-scattering geometry ($g = 128^{o}$) may result from differences between the Buz et al. (2019) and TANAGER lab setups. At the highest measurable phase angles, it is possible that TANATER's detector may receive stray light reflected from lab walls and cabinets at high emission angles. To test and potentially mitigate scattered light effects, we hung blackout curtains on the surfaces immediately adjacent to TANAGER (shown in Figure 13) and recollected the $g = 128^{o}$ spectra, which led to general decreases in overall reflectance (Figure S10) and improvements in relative RMSE values (Table 3). We now hang black curtains over all surfaces adjacent to TANAGER as part of our standard procedure.

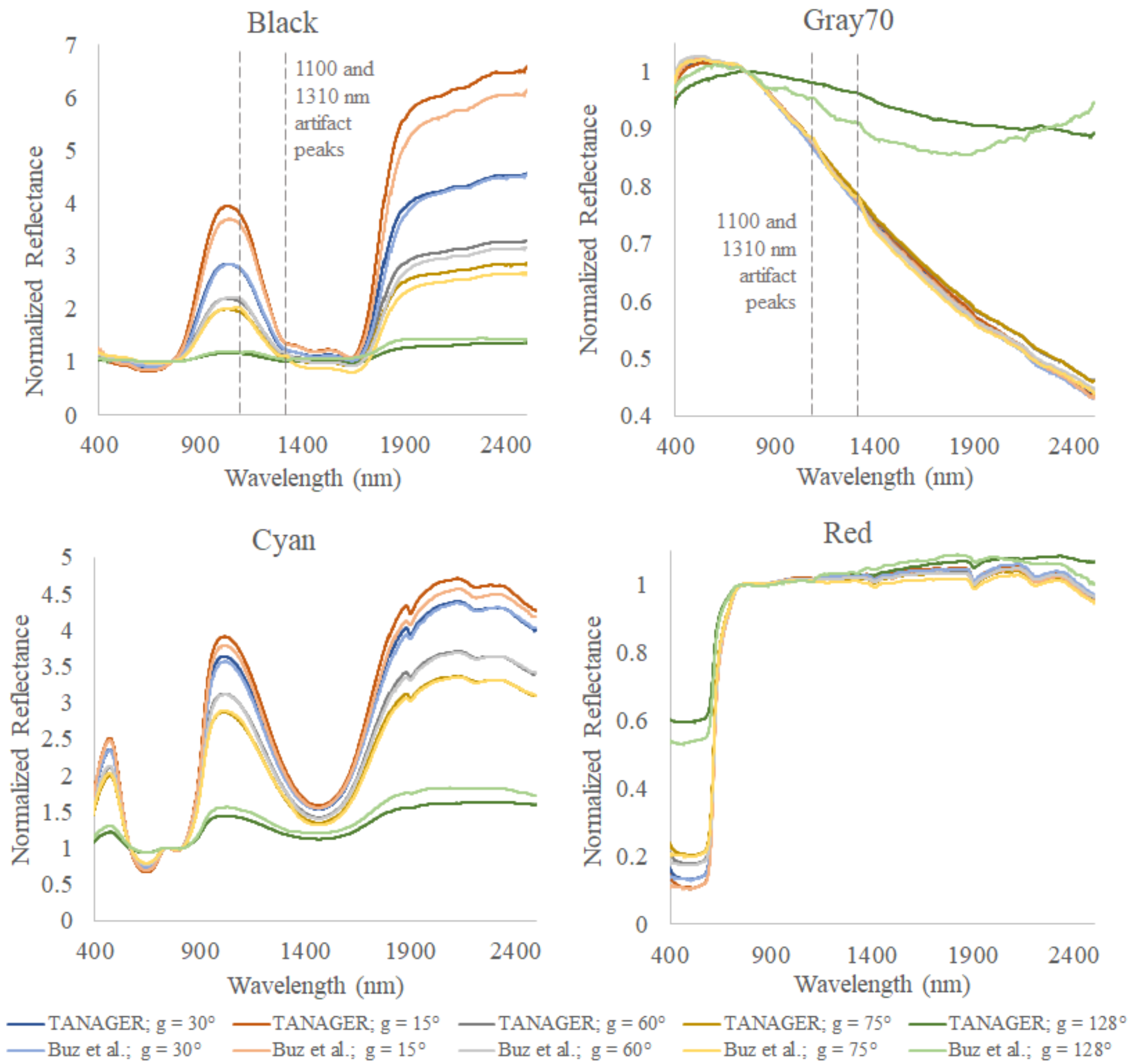

Figure 24: *Spectra normalized to 754 nm of select caltargets from TANAGER (darker lines) and Buz et al. (2019) (lighter lines) at a range of viewing geometries. Minor artifact peaks are marked in the Gray70 and Black Buz et al. (2019) spectra for g = 75° and g = 128°.*

	g = 15°	g = 30°	g = 60°	g = 75°	g = 128°	g = 128° (with black curtains)
Cyan	3.9%	1.9%	1.2%	1.3%	9.0%	4.4%
Green	4.3%	1.9%	2.0%	2.2%	8.0%	4.1%
Red	1.9%	1.3%	1.4%	1.8%	2.8%	2.9%
Yellow	1.6%	1.3%	1.4%	1.7%	3.6%	4.6%

Gray33	0.7%	1.5%	2.7%	3.4%	4.3%	3.8%
Gray70	0.9%	0.9%	1.7%	2.6%	4.2%	3.7%
Black	9.7%	3.5%	5.6%	7.9%	6.7%	5.9%
AluWhite	0.0%	0.0%	0.0%	0.0%	0.0%	0.0%

Table 3: *Relative RMSE comparing spectra normalized to 754 nm from Buz et al. (2019) and TANAGER at a range of geometries for cross calibration. Green squares have RMSE <1%, yellow-green between 1% and 3% RMSE, orange between 3% and 5% RMSE, and red above 5%. "Blackout" RMSE, right, compares Buz et al. (2019) spectra to TANAGER data collected with the addition of blackout curtains in the laboratory.*

4.2 Repeatability

The repeatability of TANAGER spectra was assessed through multiple measurements of the caltarget materials at the geometries specified in Buz et al. (2019): we compared two sets of spectra collected with TANAGER in November 2022 and February 2023. The gray and black targets have residuals < 0.01 reflectance units for all spectra except at the largest phase angles, and color target spectra are generally repeatable to within 0.02 reflectance units (Figures S11-S14). To assess repeatability of spectral shapes (as opposed to absolute reflectance), we also normalized the spectra to 1.0 at 754 nm to calculate relative RMSE (as in Section 4.1). All target-geometry combinations fall well below our 5% relative RMSE threshold, with 29 of 35 target-geometry combinations below 1% RMSE (Table 4). The very forward scattering geometry is less consistent than other geometries, but overall the data show remarkable reproducibility.

	g = 15 °	g = 30°	g = 60°	g = 75°	g = 128°
Cyan	0.4%	1.0%	0.7%	1.1%	3.5%
Green	0.4%	0.9%	0.6%	1.1%	4.2%
Red	0.3%	0.4%	0.8%	0.8%	1.1%
Yellow	0.3%	0.8%	0.7%	0.7%	2.1%
Gray33	0.2%	0.3%	0.2%	0.3%	0.9%
Gray70	0.3%	0.4%	0.5%	0.5%	0.5%

Black	0.8%	2.0%	1.0%	1.2%	0.4%
AluWhite	0.6%	0.5%	0.5%	0.5%	1.1%

Table 4: *Relative RMSE comparing duplicate runs on TANAGER normalized to 754 nm for the Caltargets at a range of geometries. Green squares have RMSE <1%, yellow-green between 1% and 3% RMSE, and orange between 3% and 5% RMSE.*

To test repeatability of spectral measurements of heterogeneous, geologic surfaces, we collected duplicate spectra at a range of phase angles from a set of four naturally-coated basalt samples from Hawaii Volcanoes National Park. All samples were collected from the Puna Coast and Mauna Iki Trails (Theuer et al., 2024) and all have brightly-colored coatings in a mottled pattern, except for MIT_LC, which has a more uniform reflective and chatoyant coating over fine-scaled flow textures (Figure 25). We documented the placement and orientation of each sample, which we referenced while resetting samples between the first and second set of spectra.

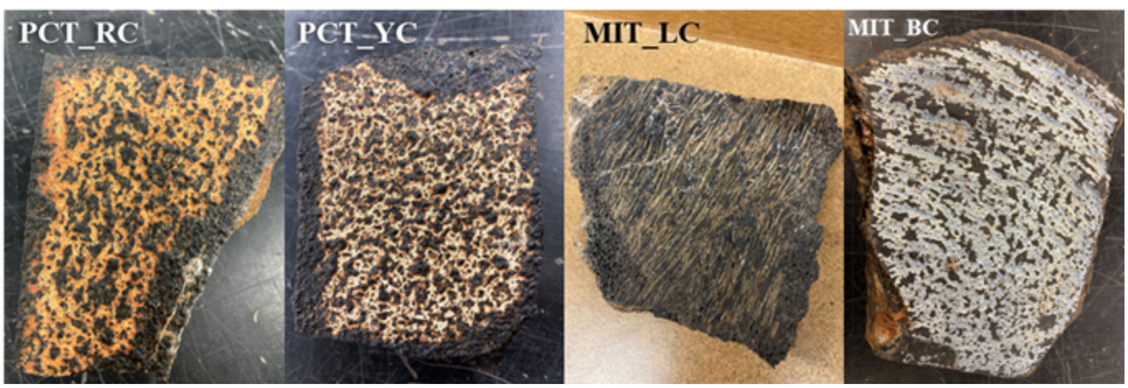

Figure 25: *Heterogeneous, naturally-coated basalts samples used to test TANAGER's measurement repeatability.*

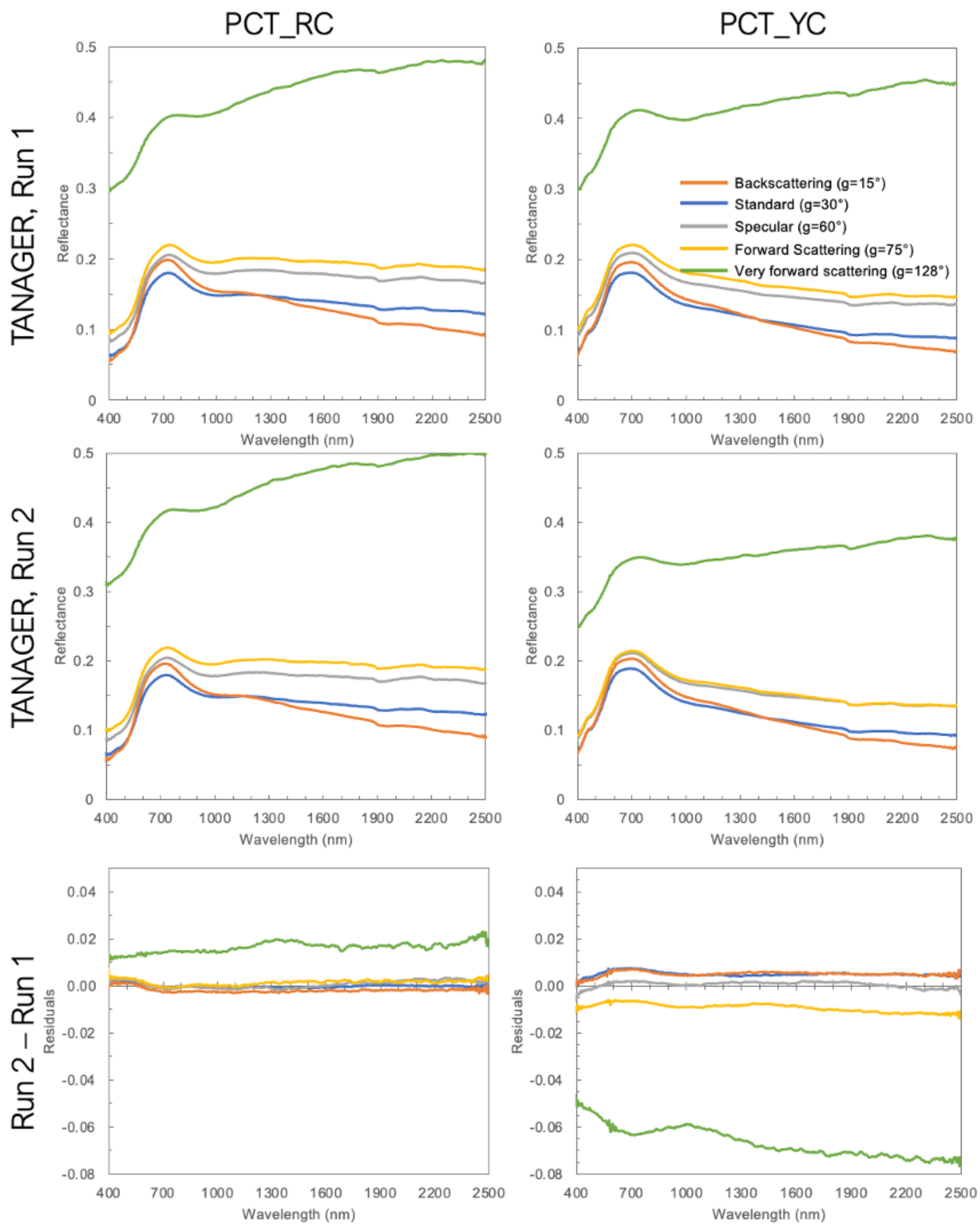

Figure 26: *Spectra of heterogenous, naturally-coated basalt samples (PCT_RC and PCT_YC, see Figure 25) from two TANAGER data collection runs (top and middle) with residuals (bottom). All measurements were acquired at i = 30º and az = 0º.*

Data from the two runs reproduce the same spectral shapes and scattering behaviors: the samples are highly forward-scattering, with substantially higher reflectances and more positive near-infrared slopes at g = 128º (Figure 26, Figure S15). For absolute reflectance spectra, residuals for most geometries are < 0.005 reflectance units. For spectra normalized to 1.0 at 754 nm, the two datasets have a relative RMSE of 3% or below (Table 9). The one exception is for the dark sample MIT_LC in the backscattering geometry, which has very low reflectance values (Figure S15). The reproducibility of TANAGER spectra for these samples gives us confidence in the consistency of both the spectrogoniomer's performance and our sample staging procedure.

	g = 15°	g = 30°	g = 60°	g = 75°	g = 128°
PCT_RC	0.6%	0.4%	1.0%	1.1%	0.4%
PCT_YC	1.5%	1.0%	1.1%	3.0%	1.1%
MIT_LC	5.6%	2.3%	2.1%	3.0%	2.1%
MIT_BC_2	2.1%	2.9%	2.2%	2.8%	0.6%

Table 9: *Relative RMSE comparing duplicate runs on TANAGER normalized to 754 nm for four coated basalt surfaces at a range of geometries. Green squares have RMSE <1%, yellow-green between 1% and 3% RMSE, orange between 3% and 5% RMSE, and red >5% RMSE.*

5. Science Applications and Data Sharing

Our preliminary science analyses have utilized TANAGER's unique design for rapid spectral measurements for large suites of natural rock surfaces, either at a single "standard" geometry (Rice et al., 2023) or over the full scattering hemisphere (Curtis, 2022; Theuer et al., 2024). Other initial studies include characterizations of multi-phase mineral mixtures (Lapo et al., 2023) and synthetic rock coatings on slabs (Gabbert et al., 2023) and sands (Gabbert et al., 2024). Because TANAGER's sample tray also accommodates SEM-mounted samples, we can easily correlate spectrogoniometric measurements with microtextural properties from backscattered electron (BSE) images and surface topography measurements (Duflot et al., 2022).

Ongoing work in the WWU Mars Lab will continue to exploit TANAGER's capabilities for interrogating natural rock surfaces. More generally, we anticipate that TANAGER's design can be useful for a variety of investigations, such as determining the bidirectional reflectance distribution function (BRDF) and deriving optical constants of minerals (e.g., Lucy, 1998; Sklute et al., 2015). We hope other laboratories will adapt TANAGER's open-source design (Hoza et al., 2023) and software (Hoza, 2023) for their own niche analyses (see Data Availability Statement).

When spectral datasets from TANAGER are published in peer-reviewed studies, we will make them available via VISOR (the [V]isible and [I]nfrared [S]pectroscopy br[o]wse[r], https://westernreflectancelab.com/visor/), an online data sharing and spectra visualization tool developed by Million Concepts, LLC in partnership with the WWU Mars Lab (Million et al., 2022). VISOR allows users to search for spectra from TANAGER and/or other published spectral databases, download spectra with associated metadata (viewing geometry and sample information), and dynamically plot user-selected spectra. Plotting capabilities include adjusting axes, normalizing spectra, applying offsets, measuring selected band depths and other spectral parameters, and convolving to the bandpasses of spacecraft multispectral cameras. We will also archive all published TANAGER datasets via third party repositories (e.g., https://zenodo.org/ or https://cedar.wwu.edu/) with a digital object identifier (DOI) and persistent identifier link.

6. Conclusions

TANAGER is a custom spectrogoniometer which is fully automated and integrated with a Malvern PanAnalytical ASD FieldSpec4 Hi-Res reflectance spectrometer. We defined TANAGER's performance requirements to enable rapid, automated spectral data collection across the full scattering hemisphere for multiple, bulky rock samples with natural surfaces. In a detailed characterization of TANAGER's performance, all defined requirements have been met. We reevaluated a selection of the performance sub-requirements after ~300 hours of use and found only minor changes to the system; we recommend frequent monitoring of some components, including laser guides and sample tray motors.

Using well-characterized color calibration targets, we have validated the accuracy of TANAGER spectra in comparison to published data. TANAGER spectra match those published from other spectrogoniometers within 5% relative RMSE, except for very low-albedo targets. In repeated TANAGER data collection runs for the same samples, we confirm that TANAGER spectra are self-consistent to within 2% in almost all instances. We also confirm that the system introduces no discernable noise or artifacts; in fact, TANAGER improves the polarization artifacts from ~1000 nm to 1400 nm that commonly occur in FieldSpec data at high phase angles. Furthermore, we find that TANGER's light source causes only minimal sample heating (+2 to 4°C over typical exposure durations) and is highly unlikely to influence sample properties such as hydration state.

The advantages of TANAGER's unique design include automation for rapid data acquisition, highly customizable viewing geometries, accommodation of multiple and/or bulky/irregular samples, and easy transfer to SEM for correlation with surface textural and compositional properties. For our near-term science analyses, TANAGER will primarily be used to characterize the surfaces of naturally-weathered rocks as analogs to the martian surface; however, TANAGER can be utilized for a variety of applications in reflectance spectroscopy. We encourage other investigators to use and/or modify TANAGER's open-source design and software for their laboratories' needs.

Acknowledgements

This work was funded as part of a NASA Solar System Working Program grant. We thank the staff of First Mode, LLC for their support in all stages of this project, including Peter Illsley, Elizabeth Frank and Sophia Kim. Western Washington University's College of Science and Engineering, Geology Department, and Machine Shop supported laboratory renovations to accommodate TANAGER. We also thank Chase Million and Michael St. Clair of Million Concepts, LLC for development and ongoing support of VISOR for data sharing. Finally, we thank the Mastcam-Z instrument team for use of the caltarget witness samples.

Data Availability Statement

TANAGER's computer-aided design (CAD), electrical schematics, and bill of materials (BOM) are publicly available as Hoza et al. (2023). TANAGER's custom software ("tanager-feeder"), which commands its motors, interfaces with the spectrometer, and visualizes the data, is open-source and available as Hoza (2023). All spectral data acquired for TANAGER's validation and characterization are available as Lapo et al. (2024).

References

Allan, A. (2011). Basic Sensors in IOS: Programming the Accelerometer, Gyroscope, and More. O'Reilly Media, Inc.

ASD Inc. (2017, September). FieldSpec4 User Guide.

J.F. Bell III, J. Joseph, J.N. Sohl-Dickstein, H.M. Arneson, M.J. Johnson, M.T. Lemmon, & D. Savransky, In-flight calibration and performance of the Mars Exploration Rover Panoramic Camera (Pancam) Instruments. J. Geophys. Res. 111, E02S03 (2006b). https://doi.org/10.1029/2005JE002444

J.F. Bell III, A. Godber, S. McNair, M.C. Caplinger, J.N. Maki, M.T. Lemmon, et al., The Mars Science Laboratory Curiosity rover Mast Camera (Mastcam) instruments: pre-flight and in-flight calibration, validation, and data archiving. Earth Space Sci. 4, 396–452 (2017). https://doi.org/10.1002/2016EA000219

Bhandari, A., Hamre, B., Frette, Ø., Zhao, L., Stamnes, J. J., & Kildemo, M. (2011). Bidirectional reflectance distribution function of Spectralon white reflectance standard illuminated by incoherent unpolarized and plane-polarized light. Applied Optics, 50(16), 2431–2442. https://doi.org/10.1364/AO.50.002431

Biliouris, D., Verstraeten, W. W., Dutré, P., Van Aardt, J. A. N., Muys, B., & Coppin, P. (2007). A Compact Laboratory Spectro-Goniometer (CLabSpeG) to Assess the BRDF of Materials. Presentation, Calibration and Implementation on Fagus sylvatica L. Leaves. Sensors, 7(9), 1846–1870. https://doi.org/10.3390/s7091846

Bishop, J. L., III, J. F. B., & Moersch, J. E. (Eds.). (2020). Remote Compositional Analysis: Techniques for Understanding Spectroscopy, Mineralogy, and Geochemistry of Planetary Surfaces. Cambridge, UK: Cambridge University Press. https://doi.org/10.1017/9781316888872

Buz, J., Ehlmann, B. L., Kinch, K., Madsen, M. B., Johnson, J. R., Rice, M. S., et al. (2019). Photometric characterization of Lucideon and Avian Technologies color standards including application for calibration of the Mastcam-Z instrument on the Mars 2020 rover. Optical Engineering, 58(02), 027108. https://doi.org/10.1117/1.OE.58.2.027108

Camon, A., & Lemelin, M. (2024). Characterizing the Spectra of Ilminite, Hematite, Mg-Spinel and Regolith Simulants to Prepare for Upcoming Lunar Missions (Vol. 55, p. Abstract 1979). Presented at the Lunar and Planetary Science Conference. Retrieved from https://www.hou.usra.edu/meetings/lpsc2024/pdf/1979.pdf

Clark, B. E., Helfenstein, P., Bell, J. F., Peterson, C., Veverka, J., Izenberg, N. I., et al. (2002). NEAR Infrared Spectrometer Photometry of Asteroid 433 Eros. Icarus, 155(1), 189–204. https://doi.org/10.1006/icar.2001.6748

Clark, R. N., & Roush, T. L. (1984). Reflectance spectroscopy: Quantitative analysis techniques for remote sensing applications. Journal of Geophysical Research: Solid Earth, 89(B7), 6329–6340. https://doi.org/10.1029/JB089iB07p06329

Clark, R. N. (1999). Remote Sensing for the Earth Sciences. In A. N. Rencz (Ed.), Manual of Remote Sensing (3rd ed., Vol. 3, pp. 3–55). John Wiley and Sons, Inc.

Cloutis, E. A., Craig, M. A., Kruzelecky, R. V., Jamroz, W. R., Scott, A., Hawthorne, F. C., & Mertzman, S. A. (2008). Spectral reflectance properties of minerals exposed to simulated Mars surface conditions. Icarus, 195(1), 140–168.

Curtis, S. (2022). Spectral variability in naturally weathered rock surfaces and implications for Mars (unpublished master's dissertation). WWU Graduate School Collection 1118. Retrieved from https://cedar.wwu.edu/wwuet/1118

Duflot, S. A., Kraft, M. D., Rice, M. S., Curtis, S. A., & Lapo, K. E. (2022). Quantitative Characterization of Weathered Rock Surface Textures and Effects on VNIR

Spectrogoniometry (Vol. 53, Abstract 2368). Presented at the Lunar and Planetary Science Conference. Retrieved from https://www.hou.usra.edu/meetings/lpsc2022/pdf/2368.pdf

Fernando, J., Schmidt, F., Pilorget, C., Pinet, P., Ceamanos, X., Douté, S., et al. (2015). Characterization and mapping of surface physical properties of Mars from CRISM multi-angular data: Application to Gusev Crater and Meridiani Planum. Icarus, 253, 271–295. https://doi.org/10.1016/j.icarus.2015.03.012

Gabbert, M. D. V., Rice, M. S., Kraft, M. D., & Lapo, K. E. (2023). Visible to Near-Infrared Spectroscopy and Photometry of Synthetic Coatings on Ultramafic Rocks with Applications for Mars. (Vol. 54, Abstract 2390). Presented at the Lunar and Planetary Science Conference. Retrieved from https://www.hou.usra.edu/meetings/lpsc2023/pdf/2390.pdf

Gabbert, M. D. V., Rice, M. S., Kraft, M. D., & Lapo, K. E. (2024). Synthetic Coatings on Ultramafic Sands with Variable Angularities: Visible to Near-Infrared Spectroscopy and Applications to Jezero Crater, Mars (Vol. 55, Abstract 1788). Presented at the Lunar and Planetary Science Conference. Retrieved from https://www.hou.usra.edu/meetings/lpsc2024/pdf/1788.pdf

Guinness, E. A., Arvidson, R. E., Clark, I. H. D., & Shepard, M. K. (1997). Optical scattering properties of terrestrial varnished basalts compared with rocks and soils at the Viking Lander sites. Journal of Geophysical Research: Planets, 102(E12), 28687–28703. https://doi.org/10.1029/97JE03018

Hapke, B. (1993). Theory of Reflectance and Emittance Spectroscopy (2nd ed.). New York: Cambridge University Press.

Hayes, A. G., Corlies, P., Tate, C., Barrington, M., Bell, J. F., Maki, J. N., et al. (2021). Pre-Flight Calibration of the Mars 2020 Rover Mastcam Zoom (Mastcam-Z) Multispectral, Stereoscopic Imager. Space Science Reviews, 217(2), 29. https://doi.org/10.1007/s11214-021-00795-x

Hoza, K. (2019, June). Photometric investigations of weathering rinds and coatings with implications for Mars (M.S.). Western Washington University, Bellingham, WA. Retrieved from https://cedar.wwu.edu/wwuet/921

Hoza, K. (2023). westernmarslab/tanager-feeder (v1.0.0). Zenodo. https://doi.org/10.5281/zenodo.8161157

Hoza, K., Kim. Sophia, Illsley, P., & Karch, J. (2023). westernmarslab/tanager-design (v1.0.0). Zenodo. https://doi.org/10.5281/zenodo.8161143

Hoza, K. M., & Rice, M. S. (2019). An Automated Goniometer System for Reflectance Spectroscopy (Vol. 50, p. Abstract 2958). Presented at the Lunar and Planetary Science Conference. Retrieved from https://www.hou.usra.edu/meetings/lpsc2019/pdf/2958.pdf

Johnson, J. R., Kirk, R., Soderblom, L. A., Gaddis, L., Reid, R. J., Britt, D. T., et al. (1999). Preliminary results on photometric properties of materials at the Sagan Memorial Station, Mars. Journal of Geophysical Research: Planets, 104(E4), 8809–8830. https://doi.org/10.1029/98JE02247

Johnson, J. R., Grundy, W. M., Lemmon, M. T., Bell III, J. F., Johnson, M. J., Deen, R. G., et al. (2006a). Spectrophotometric properties of materials observed by Pancam on the Mars Exploration Rovers: 1. Spirit. Journal of Geophysical Research: Planets, 111(E2). https://doi.org/10.1029/2005JE002494

Johnson, J. R., Grundy, W. M., Lemmon, M. T., Bell III, J. F., Johnson, M. J., Deen, R., et al. (2006b). Spectrophotometric properties of materials observed by Pancam on the Mars Exploration Rovers: 2. Opportunity. Journal of Geophysical Research: Planets, 111(E12). https://doi.org/10.1029/2006JE002762

Johnson, J. R., Grundy, W. M., Lemmon, M. T., Liang, W., Bell, J. F., Hayes, A. G., & Deen, R. G. (2021). Spectrophotometric properties of materials observed by Pancam on the Mars Exploration Rovers: 4. Final mission observations. Icarus, 357, 114261. https://doi.org/10.1016/j.icarus.2020.114261

Johnson, J. R., Grundy, W. M., Lemmon, M. T., Liang, W., Bell, J. F., Hayes, A. G., & Deen, R. G. (2022). Spectrophotometric properties of materials from the Mars Science Laboratory at Gale crater: 1. Bradbury Landing to Cooperstown. Planetary and Space Science, 222, 105563. https://doi.org/10.1016/j.pss.2022.105563

K.M. Kinch, M.B. Madsen, J.F. Bell III., J.N. Maki, Z. Bailey, A.G. Hayes, et al. (2020), Radiometric calibration targets for the Mastcam-Z Camera on the Mars 2020 Rover mission. Space Sci. Rev. https://doi.org/10.1007/s11214-020-00774-8

Kharutskiy, D. (2014). Vibration Analysis (Version 4) [IPhone Application]. Retrieved from https://apps.apple.com/us/app/vibration-analysis/id817385888

Lapo, K. E. (2021, March 5). Martian Spectroscopy: Laboratory calibration of the Perseverance rover's Mastcam-Z and photometric investigation of Mars-analog ferric-coated sand (M.S.). Western Washington University, Bellingham, WA. Retrieved from https://cedar.wwu.edu/wwuet/1011

Lapo K. E., Rice, M. S., Eng, A. M., & Curtis, S. A. (2023). VNIR Spectral Masking Effects of Hematite on Mafic Mars Analogs (Vol. 54, Abstract 1746). Presented at the Lunar and Planetary Science Conference. Retrieved from https://www.hou.usra.edu/meetings/lpsc2023/pdf/1746.pdf

Lapo, K. E., Hoza, K., Theuer, S. & Rice, M. S. (2024). Reflectance spectroscopy datasets for the validation of TANAGER. Geology Faculty Publications, 107. https://doi.org/10.25710/qzzg-bp63

Lévesque, M. P., & Dissanska, M. (2016). Field spectrometer measurement errors in presence of partially polarized light; evaluation of ground truth measurement accuracy. Optics Express, 24(24), 27199. https://doi.org/10.1364/OE.24.027199

Lichtenberg, K. A., Arvidson, R. E., Poulet, F., Morris, R. V., Knudson, A., Bell, J. F., et al. (2007). Coordinated analyses of orbital and Spirit Rover data to characterize surface materials on the cratered plains of Gusev Crater, Mars. Journal of Geophysical Research: Planets, 112(E12). https://doi.org/10.1029/2006JE002850

Lucey, P. G. (1998). Model near-infrared optical constants of olivine and pyroxene as a function of iron content. Journal of Geophysical Research, 103(E1), 1703–1713. https://doi.org/10.1029/97JE03145

Million, C. C., St. Clair, M., Rice, M. S., & Vaughan, A. (2022). Software Tools for Rapid Analysis of Mastcam-Z Multispectral Data (Vol. 53, Abstract 2533). Presented at the Lunar and Planetary Science Conference. Retrieved from http://www.hou.usra.edu/meetings/lpsc2022/pdf/2533.pdf

Painter, T., Paden, B., & Dozier, J. (2003). Automated spectro-goniometer: A spherical robot for the field measurement of the directional reflectance of snow. Review of Scientific Instruments, 74(12), 5179–5188. https://doi.org/10.1063/1.1626011

Pilorget, C., Fernando, J., Ehlmann, B. L., Schmidt, F., & Hiroi, T. (2016). Wavelength dependence of scattering properties in the VIS–NIR and links with grain-scale physical and compositional properties. Icarus, 267, 296–314. https://doi.org/10.1016/j.icarus.2015.12.029

Pommerol, A., Thomas, N., Jost, B., Beck, P., Okubo, C., & McEwen, A. S. (2013). Photometric properties of Mars soils analogs. Journal of Geophysical Research: Planets, 118(10), 2045–2072. https://doi.org/10.1002/jgre.20158

Potin, S., Brissaud, O., Beck, P., Schmitt, B., Magnard, Y., Correia, J.-J., et al. (2018). SHADOWS: a spectro-gonio radiometer for bidirectional reflectance studies of dark meteorites and terrestrial analogs: design, calibrations, and performances on challenging surfaces. Applied Optics, 57(28), 8279–8296. https://doi.org/10.1364/AO.57.008279

Rice, M. S., Johnson, J. R., Million, C. C., St. Clair, M., Horgan, B. N., Vaughan, A., et al. (2023). Spectral variability of rocks and soils on the Jezero crater floor: A summary of multispectral observations from Perseverance's Mastcam-Z instrument. Journal of Geophysical Research: Planets, 128(10), e2022JE007548. https://doi.org/10.1029/2022JE007548

Schmidt, F., & Fernando, J. (2015). Realistic uncertainties on Hapke model parameters from photometric measurement. Icarus, 260, 73–93. https://doi.org/10.1016/j.icarus.2015.07.002

Schröder, S. E., & Keller, H. U. (2009). The unusual phase curve of Titan's surface observed by Huygens' Descent Imager/Spectral Radiometer. Planetary and Space Science, 57, 1963-1974. https://doi.org/10.1016/j.pss.2009.03.012.

Shaw, A., Daly, M. G., Cloutis, E., Basic, G., Hamilton, D., Tait, K., et al. (2016). Reflectance properties of grey-scale Spectralon® as a function of viewing angle, wavelength, and polarization. International Journal of Remote Sensing, 37(11), 2510–2523. https://doi.org/10.1080/01431161.2016.1182664

Shepard, M. K. (2017). Introduction to Planetary Photometry. Cambridge: Cambridge University Press. https://doi.org/10.1017/9781316443545

Shepard, M. K., & Arvidson, R. E. (1999), The Opposition Surge and Photopolarimetry of Fresh and Coated Basalts, Icarus, 10.1006/icar.1999.6150, 141, 1, (172-178).

Shepard, M. K., & Helfenstein, P. (2007). A test of the Hapke photometric model. Journal of Geophysical Research: Planets, 112(E3). https://doi.org/10.1029/2005JE002625

Shkuratov, Y., Starukhina, L., Hoffmann, H., & Arnold, G. (1999). A Model of Spectral Albedo of Particulate Surfaces: Implications for Optical Properties of the Moon. Icarus, 137(2), 235–246. https://doi.org/10.1006/icar.1998.6035

Sklute, E. C., Glotch, T. D., Piatek, J. L., Woerner, W. R., Martone, A. A., & Kraner, M. L. (2015). Optical constants of synthetic potassium, sodium, and hydronium jarosite. American Mineralogist, 100(5–6), 1110–1122. https://doi.org/10.2138/am-2015-4824

Stack, K. M., & Milliken, R. E. (2015). Modeling near-infrared reflectance spectra of clay and sulfate mixtures and implications for Mars. Icarus, 250, 332–356. https://doi.org/10.1016/j.icarus.2014.12.009

Theuer, S. A., Rice, M. S., Kraft, M. D., Mulcahy, S. R., Lapo, K. E., Garczynski, B. et al. (2024). Characterization and the Spectral and Photometric Behavior of Mars Analog Coated Hawaiian Basalt (Vol. 55, Abstract 2546). Presented at the Lunar and Planetary Science Conference. Retrieved from https://www.hou.usra.edu/meetings/lpsc2024/pdf/2546.pdf

Veverka, J., Helfenstein, P., Hapke, B., & Goguen, J. (1989). Photometry and polarimetry of Mercury. In Mercury (pp. 37–58). University of Arizona Press. https://doi.org/10.2307/j.ctv1v090nx.7